



HAL
open science

A grid of NLTE corrections for magnesium and calcium in late-type giant and supergiant stars: application to Gaia.

Thibault Merle, Frédéric Thévenin, Bernard Pichon, Lionel Bigot

► **To cite this version:**

Thibault Merle, Frédéric Thévenin, Bernard Pichon, Lionel Bigot. A grid of NLTE corrections for magnesium and calcium in late-type giant and supergiant stars: application to Gaia.. Monthly Notices of the Royal Astronomical Society, 2011. hal-00612647

HAL Id: hal-00612647

<https://hal.science/hal-00612647>

Submitted on 29 Jul 2011

HAL is a multi-disciplinary open access archive for the deposit and dissemination of scientific research documents, whether they are published or not. The documents may come from teaching and research institutions in France or abroad, or from public or private research centers.

L'archive ouverte pluridisciplinaire **HAL**, est destinée au dépôt et à la diffusion de documents scientifiques de niveau recherche, publiés ou non, émanant des établissements d'enseignement et de recherche français ou étrangers, des laboratoires publics ou privés.

A grid of NLTE corrections for magnesium and calcium in late-type giant and supergiant stars: application to *Gaia*

T. Merle^{*}, F. Thévenin, B. Pichon, L. Bigot

*Université de Nice Sophia-antipolis; CNRS; Observatoire de la Côte d'Azur, Laboratoire Cassiopée
B.P. 4229, 06304 Nice Cedex 4, France*

Accepted ?. Received ?; in original form ?

ABSTRACT

We investigate NLTE effects for magnesium and calcium in the atmospheres of late-type giant and supergiant stars. The aim of this paper is to provide a grid of NLTE/LTE equivalent width ratios W/W^* of Mg and Ca lines for the following range of stellar parameters: $T_{\text{eff}} \in [3500, 5250]$ K, $\log g \in [0.5, 2.0]$ dex and $[\text{Fe}/\text{H}] \in [-4.0, 0.5]$ dex. We use realistic model atoms with the best physics available and taking into account the fine structure. The Mg and Ca lines of interest are in optical and near IR ranges. A special interest concerns the lines in the *Gaia* spectrograph (RVS) wavelength domain [8470, 8740] Å. The NLTE corrections are provided as function of stellar parameters in an electronic table as well as in a polynomial form for the *Gaia*/RVS lines.

Key words: line: formation, radiative transfer, stars: late-type, stars: atmospheres, stars: abundances.

1 INTRODUCTION

Individual stars of different ages carry information that allow astronomers to detail the sequence of events which built up the Galaxy. Calcium (Ca) and magnesium (Mg) are key elements for the understanding of these events since these α -elements are mainly produced by supernovae of type II. Therefore, they are both important tracers to derive trends of chemical evolution of the Galaxy. These two elements are easily observed in spectra of late-type stars through strong or weak lines. Among them, there are the Mg I b green triplet, the Ca I red triplet and the Ca II IR triplet (CaT) lines which are measurable in the most extreme metal-poor stars (Christlieb et al. 2002) even at moderate spectral resolutions.

The lines of these α -elements provide diagnostic tools to probe a wide range of astrophysical mechanisms in stellar populations. The study of α -element synthesis in halo metal-poor stars constrains the rate of SNe II (Nakamura et al. 1999). The Mg element is a reliable reference of the early evolutionary time scale of the Galaxy (e.g. Cayrel et al. 2004, Gehren et al. 2006 and Andrievsky et al. 2010). Moreover, the Ca I triplet at $\lambda\lambda$ 6102, 6122 and 6162, can be used as a gravity indicator in detailed analyses of dwarf and subgiant stars (Cayrel et al. 1996). Two Ca lines of different ionization stages can also be used to constraint surface gravity in

extremely metal-poor stars (Ca I 4226 Å and Ca II 8498 Å) as shown by Mashonkina et al. (2007). Moreover, the line strengths of CaT lines can be used as metallicity indicator for stellar population in distant galaxies (Idiart et al. 1997) or to search for the most extreme metal-poor stars in the vicinity of nearby dwarf spheroidal galaxies (Starkenburger et al. 2010). The CaT lines are also used to probe stellar activity by the measure of the central line depression as done by Andretta et al. (2005) and Busà et al. (2007).

It is well known that the assumption of Local Thermodynamic Equilibrium (LTE) is the main source of uncertainties (after the quality of the atomic data). In his review, Asplund (2005) summarized the need to take Non-LTE (NLTE) effects into account to get reliable and precise chemical abundances. Such effects are crucial in the atmospheres of metal-poor stars due to several mechanisms: the overionization in the presence of a weak opacity, the photon pumping and the photon suction. However, since the NLTE computations are still time consuming as soon as we deal with realistic model atoms, most of the studies are still done under the LTE assumption for large surveys (e.g., Edvardsson et al. 1993 for late-type dwarf stars, Liu et al. 2010 and De Silva et al. 2011 for late-type giant and subgiant stars).

Several studies of NLTE effects on Mg I lines were performed for stars of various metallicities (Mashonkina et al. 1996; Zhao et al. 1998, 2000; Gratton et al. 1999; Shiman-skaya et al. 2000; Idiart & Thévenin 2000; Mishenina et al.

* E-mail: thibault.merle@oca.eu (TM)

2004; Andrievsky et al. 2010). All studies showed an increase of NLTE effects with decreasing metallicity which imply corrections up to +0.2 dex. The first attempt to build a realistic model atom of Mg I was performed by Carlsson et al. (1992) to explain the Mg I solar emission lines near to 12 μm . They demonstrated the photospheric nature of these lines by using the photon suction mechanism which required a model atom with Rydberg states to ensure the collisional-dominated coupling with the ionization stage. The most complete Mg model atom was built by Przybilla et al. (2001) with 88 energy levels for Mg I and 37 levels for Mg II. However, they did not take into account the fine structure of the triplet system. The first Mg I model atom that includes the fine structure was built by Idiart & Thévenin (2000) who applied it to the determination of the Mg abundance for more than two hundred late-type stars. We can mention an update of the Mg I model atom of Carlsson et al. (1992) done by Sundqvist et al. (2008) in order to reproduce IR emission lines in K giants, taking into account the electronic collisions between states with the principal quantum number $n \leq 15$.

NLTE effects on Ca were investigated by Jørgensen et al. (1992) who gave a relation between equivalent widths of CaT lines as functions of the surface gravities and the effective temperatures. As for the Mg I, Idiart & Thévenin (2000) included the fine structure in their model atom of Ca I. They combined these results to the NLTE Fe abundance predictions (Thévenin & Idiart 1999) and performed an NLTE analysis of the same set of late-type dwarf and subgiant stars. They concluded that the [Ca/Fe] remained mostly unchanged but some parallel structures appeared in the NLTE [Ca/Fe] vs [Fe/H] diagram. The most complete Ca atom was done by Mashonkina et al. (2007) who built a model atom through two ionization stages with 63 energy levels for Ca I and 37 levels for Ca II, including fine structure only for the first states. They used the most recent and accurate atomic data from the Opacity Project (Seaton 1994). They concluded that NLTE abundance corrections can be as large as 0.5 dex (for the Ca I 4226 Å resonance line) in extremely metal-poor stars. Using these NLTE corrections, Asplund et al. (2009) found good agreement of solar Ca I and Ca II abundances.

In the view of the ESA *Gaia* mission (Wilkinson et al. 2005), it is important to investigate such NLTE abundance corrections in order to distinguish different stellar populations. The onboard spectrograph, named RVS (Radial Velocity Spectrometer, Katz et al. 2004) which was designed primarily to get the radial velocities can also be used in principle to extract individual chemical abundances. The spectral window considered was selected in the near-infrared [8470-8740] Å because of the presence of the CaT lines which will be visible even in the most metal-poor stars and at a considered low resolution ($R \sim 11500$ at best). The counterpart ground-based observations is the RAVE survey (Steinmetz et al. 2006) which will provide about 1 million of spectra. These two surveys will analyze a representative sample of stars throughout the Galaxy, allowing an unprecedented kinematic and chemical study of the stellar populations. The huge amount of stars will prevent us to analyze them one by one. It is necessary to have precalculated correction tables that can be used for automatic stellar parameter determination and this is the aim of this work.

The structure of the paper is as follows: in Sect. 2, we

present the model atoms of Mg I, Ca I and Ca II. In Sect. 3, we test these models by comparing NLTE synthetic lines with several solar (Sect. 3.1) and Arcturus (Sect. 3.2) lines of Mg I and Ca II in the *Gaia*/RVS region. Then, in Sect. 4.1, we present a grid of NLTE corrections of equivalent widths of spectral lines, selected in Sect. 4.2, useful for the *Gaia* mission and the RAVE survey. The behaviours of Mg I, Ca I and Ca II NLTE lines, the comparisons with previous works, the estimate of uncertainties on atomic data, and the polynomial fits of the *Gaia*/RVS lines are discussed in Sect. 4.

2 Mg I, Ca I AND Ca II MODEL ATOMS

The construction of a model atom consists in collecting and computing atomic data which are:

- the excited states of the atom characterized by their energy levels and their statistical weights;
- the radiative transitions characterized by the oscillator strength values f for the bound-bound transitions, and by the photoionization cross-sections for the bound-free ones;
- the collisional transitions with electrons and neutral hydrogen characterized by the collisional strength Ω ;
- the elastic radiations and collisions with neutral hydrogen characterized by the radiative (γ_{rad}) and the collisional (γ_{coll}) damping factors.

2.1 Construction of model atoms

Energy levels. The energy levels come from the NIST¹ (Ralchenko et al. 2008) and the TopBase² (Cunto & Mendoza 1992) on line atomic databases. When theoretical levels are present in the TopBase but absent in the NIST, we add them in the model atoms by shifting them with respect to the NIST ionization energies. We consider the fine structure of energy levels as long as they exist in NIST database. If some fine levels are missing for the highest levels in atomic databases, we compute them as specified in the next subsections.

Radiative transitions. The oscillator strengths of bound-bound transitions considered here are from VALD³ (Kupka et al. 2000), Kurucz⁴ (Kurucz & Bell 1995) and NIST on line databases. We take the VALD log gf values as default for the whole transitions of an atom and choose the most accurate one among VALD, NIST, Hirata & Horaguchi (1995), and Kurucz for the selected lines. For the bound-free transitions, we use the theoretical tables of photoionization cross-sections provided by the TopBase. We shift the TopBase energy threshold of photoionization to the corresponding NIST values to keep consistency with the measured NIST energy levels. In order to save computational time, we undersampled the photoionization cross-section tables taking care to keep large resonance peaks near the photoionization threshold but smoothing faint peaks far from the threshold using

¹ available at: <http://physics.nist.gov/asd3>

² available at: <http://cdsweb.u-strasbg.fr/topbase/topbase.html>

³ available at: <http://vald.astro.univie.ac.at>

⁴ available at:

<http://www.cfa.harvard.edu/amp/ampdata/kurucz23/sekur.html>

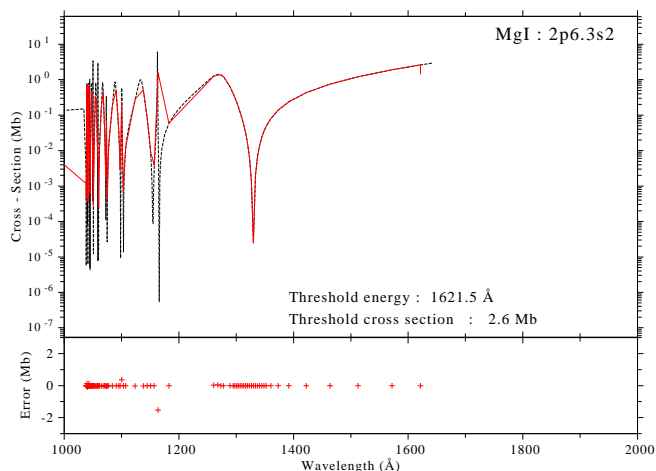


Figure 1. Photoionization cross-section as a function of the energy of the incident photon for the $3s^2\ ^1S$ ground state of Mg I. We use a slide window to smooth data after the resonance peak and undersample them. Dashed line stands for data from Top-Base, red full line stands for smoothed and undersampled data used in our atomic model.

a slide window (see Fig. 1). We assume that the photoionization cross-sections are the same for the fine structure of a level. Some photoionization data are missing for high levels, therefore we calculated photoionization threshold using hydrogenic cross-section formulation of Karzas & Latter (1961), allowing us to compute Gaunt’s factor as functions of the quantum numbers n and l . This approach leads to a better estimation than the standard formulation of Menzel & Pekeris (1935) and Mihalas (1978).

Collisional transitions. The inelastic collisions between the considered atoms with the other particles of the medium tend to set the atom in the Boltzmann Statistical Equilibrium (SE). A careful treatment of these collisional transitions is therefore important for the SE that defines the level populations. Tables of quantum calculations of the collisional cross-sections with electrons are implemented when available. Otherwise, we use the modified Impact Parameter Method (IPM) of Seaton (1962a) for allowed bound-bound collisions with electrons, which uses values of oscillator strengths corresponding to radiative ones, and depends on the electronic density and temperature structures of the model atmosphere. Seaton (1962a) emphasized that the collisional rates are more reliable when $(13.6/\Delta E)f$ is large, where ΔE is the energy of the transition in eV. Then, for intercombination lines with low f values, the collisional rate can be under-estimated. For the forbidden transitions, when no quantum computations are available, it is generally assumed that the collisional strength Ω_{ij} does not depend on the energy of the colliding electrons. We choose $\Omega_{ij} = 1$ (as in Allen 1973 and Zhao et al. 1998) since quantum calculations give this order of magnitude for some forbidden optical lines (e.g. Burgess et al. 1995). For forbidden transitions between fine levels, we choose $\Omega_{ij} = 10$ in order to couple them by collisions. Collisional ionization with electrons are computed following Seaton (1962b) in Mihalas (1978) where the collisional ionization rates are taken to be proportional to the photoionization cross-sections.

It is known today that the inelastic collisional cross-sections with neutral hydrogen atoms are largely over-

estimated by the Drawin’s formula (Drawin 1968) when applied to dwarf stars (see Caccin et al. 1993, Barklem et al. 2003, Barklem et al. 2011). This over-estimation tends to force LTE by exaggerating the collisional rates with respect to the radiative ones. For giant and supergiant stars that we consider in this paper, we assume, *a priori*, that the low gas density in the atmospheres of these stars make the H-collisions inefficient. Note that for the Mg I and Ca I atoms efforts are being made to compute with quantum mechanics the exact cross-sections for inelastic collisions with neutral hydrogen (Guitou et al. 2010). These results will be implemented in a dedicated forthcoming paper.

Damping parameters. The radiative damping is calculated using the Einstein coefficients of spontaneous de-excitation of each level present in the model atom:

$$\gamma_{\text{rad}} = \sum_{k < j} A_{jk} + \sum_{k < i} A_{ik}, \quad (1)$$

where i stands for the lower level and j for the upper level. For the collisional damping γ_{coll} , we only take into account elastic collisions with neutral hydrogen, namely the Van der Waals’ damping. Stark broadening is ignored in the present calculations, therefore: $\gamma_{\text{coll}} = \gamma_{\text{vdw}}$. We use quantum calculations of hydrogen elastic collisions with neutral species from Anstee & O’Mara (1995); Barklem & O’Mara (1997); Barklem, O’Mara & Ross (1998), hereafter named ABO theory. The great improvement of quantum mechanical calculation compared with the traditional Unsöld recipe (Unsöld 1955) is to lead to line widths that agree well with the ones observed without the need of an adjustable factor F_H (e.g. Mihalas 1978; Thévenin 1989). As used later in Table 3 and 4, we translate results from the ABO theory in terms of an enhancement factor F_H which is the ratio between ABO broadening and classical Unsöld broadening. We notice that for transitions including terms higher than $l \geq 4$ no broadening parameters are available from ABO theory. For these lines, we use an averaged value of this enhancement factor $F_H = 2$. We tested several values in the range of 1 to 4 and found no significant effect on the resulting NLTE over LTE equivalent width ratios.

2.2 Magnesium model atoms

We developed two models for the neutral Mg atom:

- one for the lines outside the *Gaia*/RVS wavelength range (model A) with the detailed fine structure of the energy levels;
- one dedicated to the multiplets in the *Gaia*/RVS wavelength range (model B) which need a special treatment to account for the blended multiplets rather than the separated components.

2.2.1 Mg I model atom A

Since the neutral Mg is an alkaline earth metal, its electronic configuration leads to a singlet and a triplet systems. We consider all levels until $n = 10$ and $l = 9$ with fine structure for all levels with $l \leq 4$. For levels with $l > 4$, the multiplicity systems are merged (for the H , I , K , L and M terms) and no fine structure is considered. For completeness and because some high energy levels are missing in the

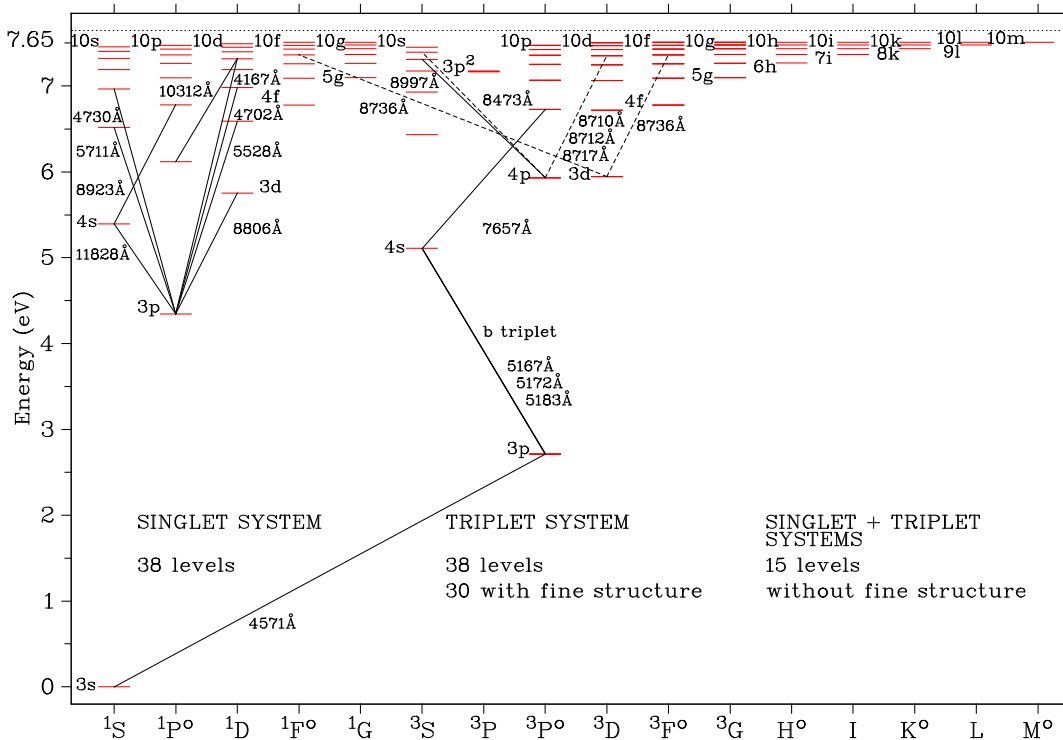


Figure 2. Mg I Grotrian diagram. The electronic configuration of the ground state is $[\text{Ne}]3s^2$. Two multiplicity systems are present due to spin combination of the incomplete sub-level $n = 3$. All levels with fine structure are complete until $n = 10$ and $l = 4$ (but not visible at this scale); fine levels and multiplicity systems were merged for $5 \leq l \leq 9$. Only one doubly-excited state $3p^2$ is present in triplet system since in the singlet system the value of the corresponding energy level is greater than the ionization stage of Mg I. Horizontally dotted line stands for the ionization stage. Transitions represented by solid lines are those for which we deliver NLTE corrections; transitions represented by dashed lines are those in the *Gaia*/RVS wavelength range.

databases, we used the formulation of polarization theory given by Chang & Noyes (1983) to include them. We take into account 38 spectral terms in the singlet system and 38 in the triplet system plus 15 merged terms (singlet + triplet systems without fine structure). In total, 149 energy levels + ionization stage (at 7.646 eV) are considered for the SE computation (see the Grotrian diagram in Fig. 2).

1102 radiative bound-bound transitions have been taken into account: 127 allowed in the singlet system, 674 in the triplet system and 301 intercombination transitions (semi-allowed transitions between the two systems). We used hydrogenic approximation (Green et al. 1957) to compute several $\log gf$ missing in VALD. For transitions between levels with and without explicit fine structure, we did two assumptions to estimate individual oscillator strengths: firstly, as the transitions are produced between Rydberg states, the wavelength shifts between components are small enough to be neglected; and secondly the oscillator strength of each component of one multiplet is given in the LS coupling. The TopBase photoionization cross-sections come from Butler et al. (1993). 11026 electronic collisions between all levels and sub-levels are included using the IPM approximation when corresponding radiative transitions exist. The elastic collisional broadening from the ABO theory is interpolated for 87 transitions ($s - p$, $p - d$ and $d - f$) in singlet and triplet systems, the Unsöld recipe is used with $F_H = 2$ for the remaining transitions.

2.2.2 Mg I model atom B for the *Gaia*/RVS lines

In order to reproduce Mg I lines in *Gaia*/RVS wavelength range, we construct a second Mg I model atom which enables MULTI to compute these lines as blended multiplets rather than separate components. These lines appear in the triplet system. We merge fine levels E_i under interest taking average energy level E_{level} with respect to their statistical weights g_i :

$$E_{\text{level}} = \frac{\sum_{i=1}^3 g_i E_i^{\text{fine level}}}{\sum_{i=1}^3 g_i}, \quad (2)$$

as illustrated in Fig. 8. Averaged energy of each considered level and its fine structure are represented in Fig. 8. Then only averaged levels of $4p^3P^\circ$, $3d^3D$, $7d^3D$ and $7f^3F^\circ$ are considered in this model atom B. The radiative transfer for a multiplet is then done under assuming that the same source function is used for the components of this multiplet (Mihalas 1978). Moreover we take the oscillator strength of the multiplet as a linear combination of the weighted gf of each component (in LS coupling). Actually, we can neglect the wavelength deviation between components and multiplet (relative deviation smaller than 1% for the Mg I lines):

$$g_i f_{ij}^{\text{mult}} = \frac{1}{\lambda_{ij}} \sum_u \sum_l g_l \lambda_{ul} f_{lu} \simeq \sum_u \sum_l g_l f_{lu} \quad (3)$$

with respect to the line selection rules and with λ_{ij} (named Ritz wavelength) the average wavelength of the multiplet, $g_i = \sum_l g_l$, l for lower fine levels of term i , and u for upper

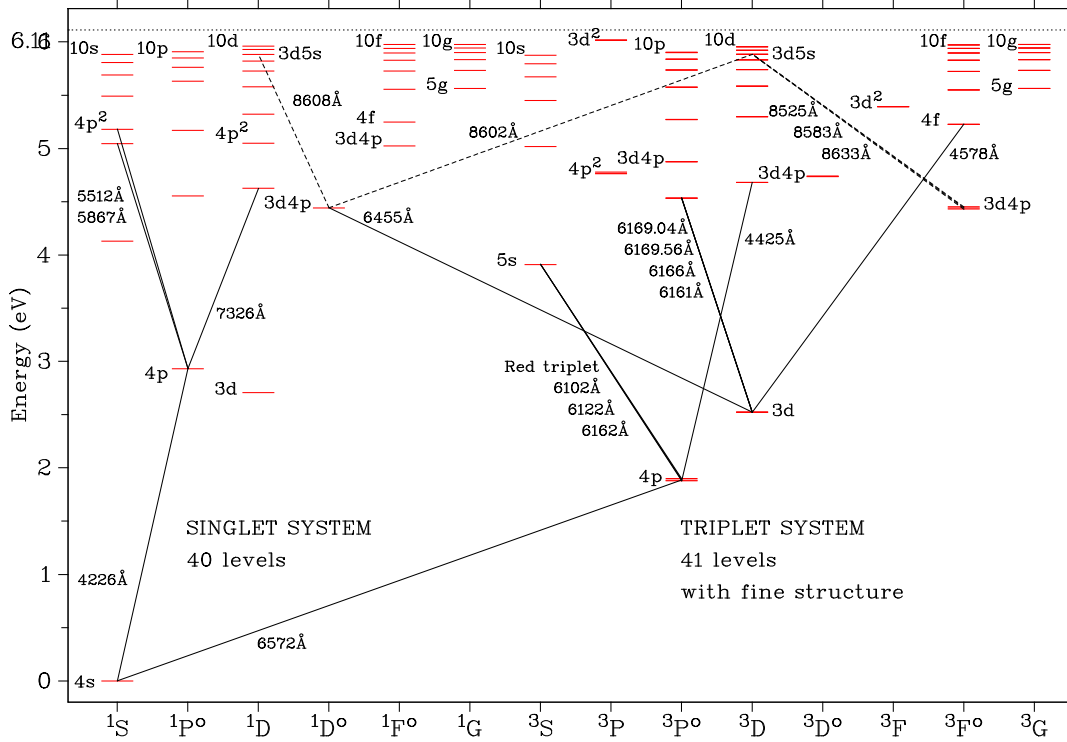


Figure 3. Ca I Grotrian diagram. The electronic configuration of the ground state is $[\text{Ar}]4s^2$. All levels with fine structure are complete until $n = 10$ and $l = 4$. Twelve doubly excited terms are present: $4p^2 \ ^1SD \ ^3P$, $3d^2 \ ^3PF$ (the terms for the singlet system 1SDG are missing but thought to be above the ionization threshold), $3d4p^1DF \ ^3PDF^o$ (the terms for the singlet system $^1P^o$ are missing) and $3d5s \ ^1D \ ^3D$. Horizontally dotted line stands for the ionization level. Transitions represented by solid lines are those for which we deliver NLTE corrections; transitions represented by dashed lines are those in the *Gaia*/*RVS* wavelength range.

fine levels of term j . We note that merging these fine levels implies shifts in wavelengths for the other lines. Then this atom will be exclusively used for the study of the lines in the *Gaia*/*RVS* wavelength range, except for the singlet line at 8473 Å for which we use the Mg I model atom A.

2.3 Calcium model atoms

The neutral and first ionized Ca model atoms are built in the same way as the Mg I model atom A, but we consider them separately. We build separate model atoms of Ca I and Ca II, but for comparison with Mashonkina et al. (2007) we merge the two separate atoms of Ca I and Ca II to have a model atom of Ca through two ionization stages.

2.3.1 Ca I model atom

Neutral Ca is also an alkaline earth metal with two multiplicity systems: singlet and triplet systems. However, more doubly excited energy levels exist which produce a more complex model atom than the Mg I one. All energy levels until $n = 10$ and $l = 4$ are considered with fine structure and we take into account all doubly excited levels under ionization stage of Ca I. This leads to consider 151 levels + ionization stage (at 6.113 eV). A Grotrian diagram is shown in Fig. 3. Twelve doubly excited levels are presented for $4p^2$, $3d^2$, $3d4p$ and $3d5s$ electronic configurations (see the legend of Fig. 3 for more details). The TopBase photoionization cross-sections come from Saraph & Storey (unpublished). All transitions

present in VALD are considered representing 2120 transitions: 191 in the singlet system, 1161 in the triplet system and 768 between these two systems. For elastic collisions with neutral hydrogen, the ABO theory provides broadening for 107 lines.

11628 electronic collisions are involved in the Ca I model atom but only 11 collisional cross-sections with electrons for resonance transitions are available from quantum computations (Samson & Berrington 2001). These authors used the Variable Phase Method (VPM) for Ca I lines shown in Table 3. For inelastic collisions with neutral hydrogen, we can refer to Mashonkina et al. (2007) who show detailed tests of the importance of these inelastic collisions. They conclude that for many transition lines these collisions are small for Ca I and negligible for Ca II to reproduce the line profiles.

2.3.2 Ca II model atom

The Ca II atom is like an alkali element, so it presents only one system of levels with a doubly multiplicity system (see Fig 4). We consider levels until $n = 10$ and $l = 5$ for Ca II. Fine structure is used, leading to 74 levels for Ca II. 422 radiative transitions are considered from the VALD database. Photoionization cross-sections from the TopBase (Saraph & Storey unpublished) do not present any peaks. In the ABO theory, the line broadening due to elastic collisions with hydrogen is only known for the H, K and CaT lines (Barklem & O'Mara 1998). 2775 inelastic collisions with electrons are involved in the Ca II model atom. Quantum computations

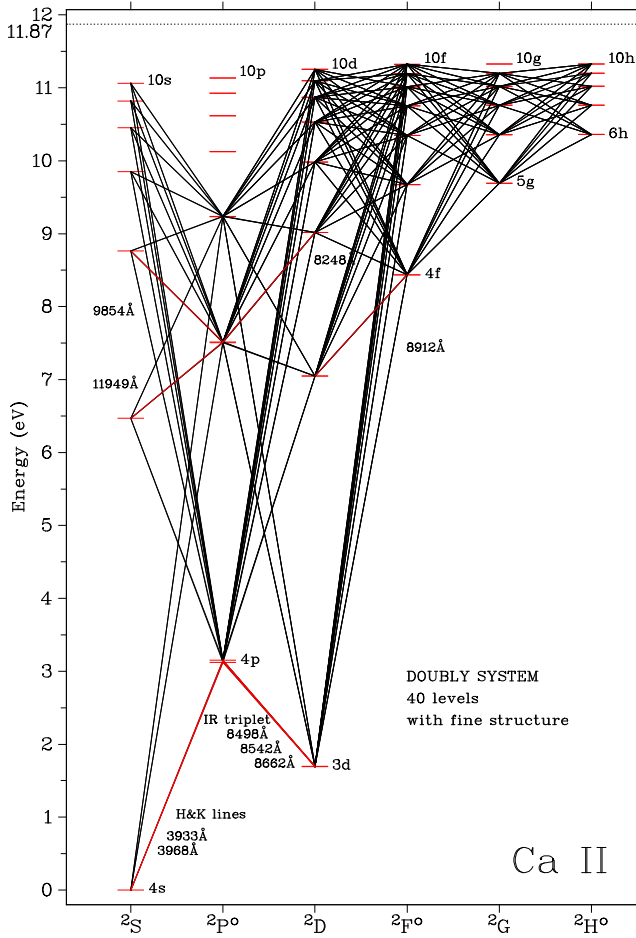


Figure 4. Ca II Grotrian diagram. First ionized calcium has a doubly multiplicity system. In this case, we have represented all the radiative bound–bound transitions used in the model atom with full lines. Transition represented by red lines are those for which we will deliver NLTE corrections. Horizontally dotted line represents the ionization stage.

are available from Burgess et al. (1995), using the Coulomb Distorted Wave approximation (CDW), for 21 transitions between mean levels: 10 allowed and 11 forbidden as reported in Table 3. For components between fine levels, we apply the same ratio from the oscillator strengths gf to the collisional strength Ω .

2.3.3 *Ca I/II model atom*

In order to see if NLTE effects act on the ionization equilibrium, we build a Ca I/II model atom by merging the Ca I and the Ca II ones. Several energy levels of Ca I are photoionized on excited levels of Ca II. It is the case for the doubly excited levels $3d4p^1DF^3PDF^o$ which photoionize on $3d^2D$ of Ca II and for the $4p^2^1SD^3P$ which photoionize on to $4p^2P^o$ of Ca II. This model atom is used to compare results with those of Mashonkina et al. (2007) in Sect. 4.4.1.

3 TEST ON TWO BENCHMARK STARS: THE SUN AND ARCTURUS

The new model atoms of these α -elements are first tested on two well known benchmark stars: a main sequence star (the Sun) and a giant (Arcturus). We compute flux profiles for several lines in the *Gaia*/RVS wavelength range using the NLTE radiative transfer code MULTI (Carlsson 1986). This code directly provides correction ratios of NLTE (W) versus LTE (W^*) equivalent widths (EW), hereafter named NLTE/LTE EW ratios or W/W^* .

We define the abundance of an element (El) relative to hydrogen by A_{El} using notation⁵ from Grevesse et al. (2007). Stellar abundances are given with respect to the solar ones on a logarithmic scale $[El/H]$ as usually done⁶. The abundances of α -elements are given with respect to iron by $[\alpha/Fe]$.

We also define NLTE abundance correction as:

$$\Delta[El/H] = A_{El}^{NLTE} - A_{El}^{LTE}, \quad (4)$$

where A_{El}^{LTE} is the LTE abundance of the element El, and A_{El}^{NLTE} the NLTE abundance.

For very weak lines (e.g. Mg I 8473 Å) or for very strong lines (e.g. CaT), one can express W/W^* as a function of the abundance ratio by using the curve of growth theory:

$$\frac{W}{W^*} = \left(\frac{A_{El}^{NLTE}}{A_{El}^{LTE}} \right)^{-\beta}, \quad (5)$$

where β is a coefficient which depends on the strength of the line. If $\log(W/\lambda) \leq -4.8$, the line is considered weak and $\log(W/\lambda)$ has a linear dependence on the abundance ($\beta = 1$); if $\log(W/\lambda) \geq -4.2$ the line is considered strong and $\log(W/\lambda)$ has a square root dependence on the abundance ($\beta = 1/2$). We deduce for these two extreme cases the NLTE abundance correction as:

$$\Delta[El/H] = -\frac{1}{\beta} \log(W/W^*). \quad (6)$$

We apply this relation to deduce NLTE abundance corrections $\Delta[El/H]$ from W/W^* when we compare weak and strong lines with the available literature as done in Table 1, 6 and 9. Note that between these two extreme cases, β is lower than 1/2. This can imply strong variations of $\Delta[El/H]$ corresponding to the plateau of the curve of growth (e.g. Mihalas 1978, pp 319, 320 and 325). We emphasize that Eq. 6 is an approximation that gives an estimate of the NLTE abundance correction. The right way to determine the NLTE abundance correction should be to vary the NLTE abundance of El until the NLTE EW fits the observed EW.

In the following sections, we test our model atoms on the Sun for which we know in advance that NLTE effects are small (Asplund 2005) but that can be used to estimate the missing enhancement factor F_H for some *Gaia* lines (outside of the ABO theory range). We also test our model atoms on Arcturus, a well known red giant, using high resolution and high S/N spectrum.

⁵ $A_{El} = \log_{10}(N_{El}/N_H) + 12$, N the number density of a given element.

⁶ $[El/H] = A_{El}^* - A_{El}^\odot$.

Table 1. Solar NLTE abundance corrections for Mg I lines of astrophysical interest with ($\Delta[\text{Mg}/\text{H}]_H$, $S_H = 1$) and without ($\Delta[\text{Mg}/\text{H}]$, $S_H = 0$) inelastic collisions with neutral hydrogen according to a scaled Drawin’s formula. We applied Eq.(6) to compute $\Delta[\text{Mg}/\text{H}]$ and $\Delta[\text{Mg}/\text{H}]_H$.

λ [Å]	W [mÅ]	W_H [mÅ]	W/W^* [mÅ]	W/W_H^*	This work		Zhao et al. (1998)	
					$\Delta[\text{Mg}/\text{H}]$	$\Delta[\text{Mg}/\text{H}]_H$	$\Delta[\text{Mg}/\text{H}]$	$\Delta[\text{Mg}/\text{H}]_H$
4571.095	83	85	0.935	0.954	0.06	0.02	0.07	0.03
5167.320	675	706	0.954	0.998	0.04	0.00	0.04	0.01
5172.683	1139	1195	0.951	0.998	0.04	0.00	0.04	0.01
5183.603	1430	1502	0.949	0.998	0.05	0.00	0.04	0.01
5528.403	333	342	0.973	1.001	0.02	0.00	0.06	0.00
8806.751	465	499	0.934	1.001	0.06	0.00	0.09	-0.03
8923.563	43	47	0.929	1.001	0.03	0.00	0.11	0.02
11828.18	755	771	0.981	1.001	0.02	0.00	0.05	0.02

3.1 NLTE synthetic line profile fits of solar lines

We compare our NLTE disk integrated line profiles with the observed solar spectrum obtained by the Fourier Transform Spectrograph, here-after FTS (Brault & Neckel 1987)⁷. This is particularly well adapted for the present work because of its high signal-to-noise ratio ($S/N > 500$) and its large resolving power ($R \sim 400000$). We use a 1D, static, and plane-parallel solar model atmosphere from MARCS grid (Gustafsson et al. 2008) with $T_{\text{eff}} = 5777$ K and $\log g = 4.44$. The solar abundances of Ca and Mg are from Grevesse et al. (2007) corresponding to $A_{\text{Mg}}^{\odot} = 7.53$ and $A_{\text{Ca}}^{\odot} = 6.31$. The flux profiles are convolved with a gaussian profile to account for the effects of macroturbulence velocity (~ 2 km s⁻¹). As the projected rotational velocity is weak for the Sun, we neglect it.

The NLTE effects on lines in the visible wavelength range for both Mg I and Ca I are small in the late type solar-like stars (e.g. comparing the NLTE abundances from Idiart & Thévenin 2000 with the LTE ones from Thévenin 1998). However, NLTE effects become non-negligible for IR lines (see the conclusion of Zhao et al. 1998). As an example, we compare NLTE and LTE profiles for Mg I lines in the RVS wavelength range. In the top panel of Fig. 5, we show the Mg I 8736 Å multiplet computed with the model B. This line is fitted in NLTE with a value of $F_H = 3$ and $A_{\text{Mg}}^{\text{NLTE}} = 7.63$. We find a ratio of $W/W^* = 1.10$ and a NLTE EW of 204 mÅ. The LTE fit gives a value of $A_{\text{Mg}}^{\text{LTE}} = 7.70$. Therefore, we have $\Delta[\text{Mg}/\text{H}] = -0.07$ dex of NLTE abundance correction for this line on the Sun. The middle panel of Fig. 5 presents the Mg I triplet at $\lambda\lambda$ 8710, 8712 and 8717 computed assuming the same source function since we have merged lower and upper fine levels into one lower and one upper in model B. Our best fit is obtained with $F_H = 2.5$, $A_{\text{Mg}}^{\text{NLTE}} = 7.63$ and we found that NLTE effects are negligible for this multiplet since $W/W^* = 1.02$.

We compare our NLTE results for the Sun with Zhao et al. (1998) who used Kurucz’s model atmosphere with the DETAIL code (Butler & Giddings 1985) to perform NLTE computations. They studied the impact of the inelastic collision with hydrogen on the NLTE results, using Drawin’s formula and empirical scaling laws. We compute $\Delta[\text{Mg}/\text{H}]$ using Eq. (6) for several lines in common with their study. For the comparison, we add collisions with neutral hydrogen,

using Drawin’s formula with a scaling factor $S_H = 1$. Results are presented in Table 1 for solar lines. For the Mg I b triplet we obtain a very good agreement with Zhao et al. (1998). For other transitions, our NLTE corrections are lower than theirs. The effect of inelastic collisions with neutral hydrogen, through Drawin’s formula, eliminates completely the NLTE effects except for the intercombination resonance line at 4571 Å for which we have $\Delta[\text{Mg}/\text{H}]_H = 0.02$ (0.03 in Zhao et al. 1998). In the Sun, NLTE corrections for these lines are all less than 0.06 dex. If we do not take into account Drawin’s formula, all the NLTE corrections are positive. We have already mentioned in Sect. 2.1 that Drawin’s formula is not adapted for the inelastic collisions with neutral hydrogen.

We also consider NLTE effects on the well studied CaT. We note that the central depression of these lines are deeper in NLTE compared to LTE ones as seen in the bottom panel of Fig. 5. The discrepancies with the observations are due to the fact that the cores of these lines form in the chromosphere which is not included in the MARCS model atmospheres. Since these strong lines are dominated by the wings that are formed in LTE, the equivalent widths are quite insensitive to NLTE in solar conditions ($W/W^* \sim 1.00$). Note that the small asymmetry of the line core may be due to an isotopic shift as shown by Kurucz (2005) and Mashonkina et al. (2007) but a contribution of 3D effect is also not to be excluded.

3.2 NLTE synthetic line profile fits of Arcturus

We compute NLTE line profiles using an interpolated MARCS model atmosphere (spherical geometry, $T_{\text{eff}} = 4300$ K, $\log g = 1.5$, $[\text{Fe}/\text{H}] = -0.5$, $[\alpha/\text{Fe}] = +0.2$, $\xi = 2$ km s⁻¹, $M = 1 M_{\odot}$) obtained with the interpolation code of T. Masseron⁸. The spectrum of Arcturus comes from the Narval instrument at the Bernard Lyot Telescope⁹ ($R \sim 65000$) with high signal-to-noise ratio ($S/N > 500$).

The computation of Arcturus line profiles reveals that NLTE effects are larger than in the Sun in particular for the *Gaia*/RVS lines as shown in Fig. 6. When we fit the Mg I 8736 Å line with $A_{\text{Mg}}^{\text{NLTE}} = 6.93$, we find an equivalent width of 128 mÅ and a ratio of $W/W^* = 1.30$. The LTE fit of the same line gives a value of $A_{\text{Mg}}^{\text{LTE}} = 7.23$. Therefore, we have $\Delta[\text{Mg}/\text{H}] = -0.30$ dex of NLTE abundance correction for

⁷ available at: <ftp://ftp.hs.uni-hamburg.de/pub/outgoing/FTS-Atlas/>

⁸ available at: <http://marcs.astro.uu.se/software.php>

⁹ available at: <http://magics.bagn.obs-mip.fr>

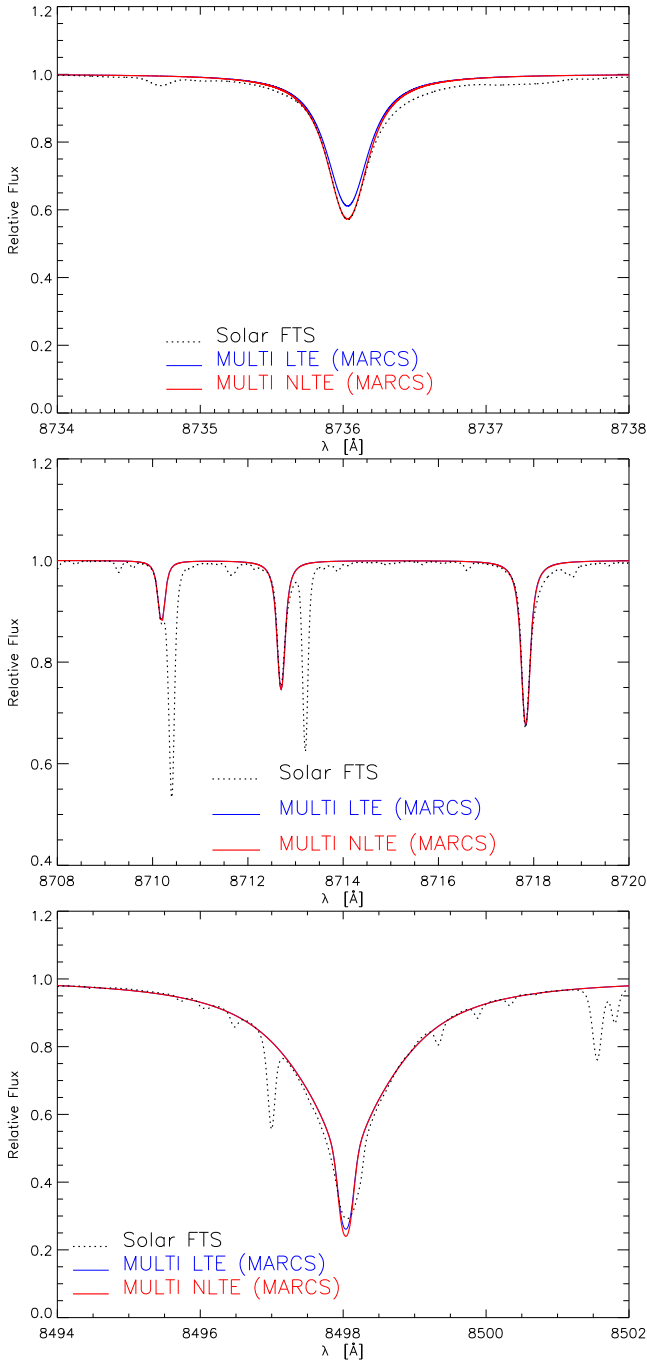


Figure 5. Solar line fits in the *Gaia*/RVS wavelength range, using a solar plane-parallel MARCS model. The blue lines stand for LTE synthesis and the red lines for NLTE synthesis. Dashed lines stand for observations. Top panel: Mg I 8736 Å multiplet. Middle panel: Mg I triplet at $\lambda\lambda$ 8710, 8712 and 8717. Bottom panel: Ca II 8498 Å line.

this line in Arcturus. For the Mg I triplet at $\lambda\lambda$ 8710, 8712 and 8717, the NLTE effects are smaller than for 8736 Å line but larger than in the Sun. We find $W/W^* = 1.10$.

Concerning the Ca II IR 8498 Å line, departure from LTE always affects the line core. We are not able to reproduce satisfactorily the observed line core, neither in LTE or NLTE as shown in bottom panel of Fig. 6. Contrary to the

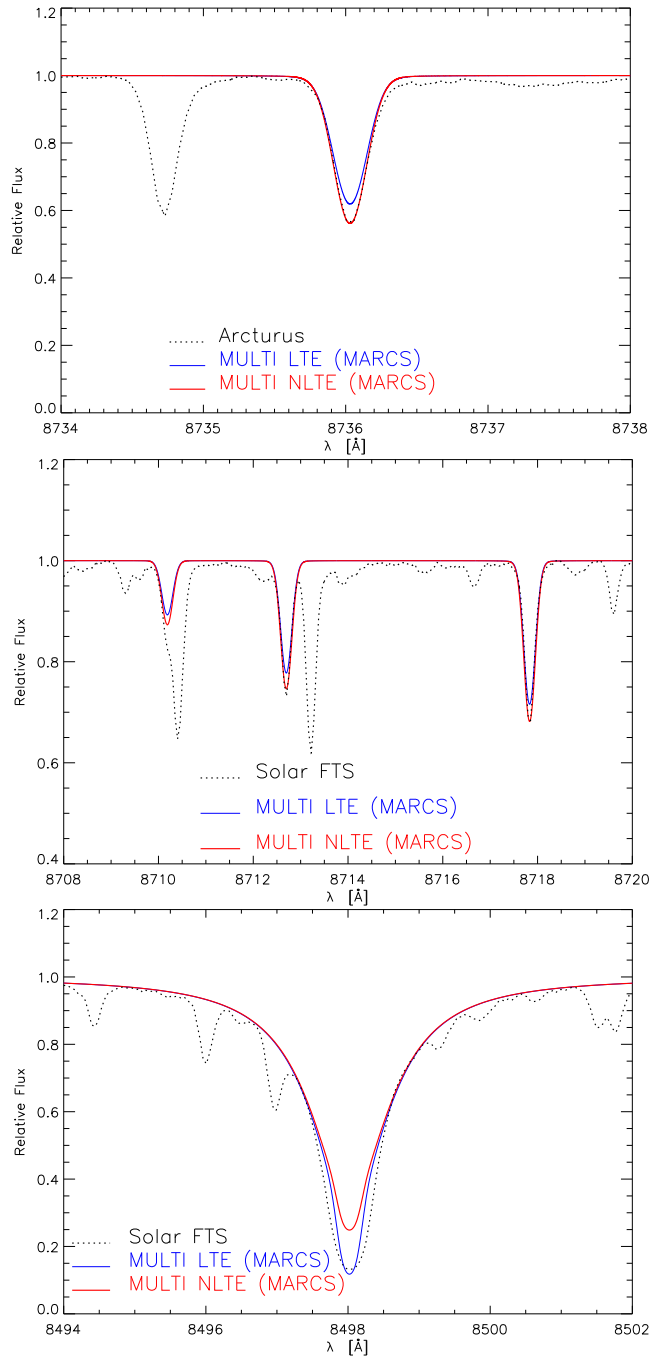


Figure 6. Arcturus line fits in the *Gaia*/RVS wavelength range, using a spherical interpolated MARCS model atmosphere. The blue lines stand for LTE synthesis and the red lines for NLTE synthesis. Dotted lines stand for observations. Top panel: Mg I 8736 Å multiplet. Middle panel: Mg I triplet at $\lambda\lambda$ 8710, 8712 and 8717. Note that NLTE effects are more pronounced than the Sun (Fig. 5). Bottom panel: Ca II 8498 Å line. Departure from LTE appears in the core.

solar case, the central depression of these lines are deeper in LTE compared to NLTE ones. The best value of Ca abundance fitting the wings of this line in NLTE is $A_{\text{Ca}}^{\text{NLTE}} = 5.81$. The equivalent width ratio is $W/W^* = 0.95$. As in the Sun, the discrepancy in the line core is probably due to the presence of a chromosphere in such giant stars and in particular in Arcturus for which many studies have been devoted (e.g. Ayres et al. 1982).

4 NLTE EFFECTS VERSUS ATMOSPHERIC PARAMETERS

We compute an NLTE correction table for a wide range of stellar parameters (T_{eff} , $\log g$, $[\text{Fe}/\text{H}]$) of cool giant and supergiant stars with metallicities from +0.5 down to -4 dex. The selected lines are those of astrophysical importance in the optical and near IR wavelength ranges, especially for those in the domain of the *Gaia*/RVS. Then, we describe the general trends of NLTE effects for the selected Mg I, Ca I and Ca II lines of astrophysical interest (Table 3 and 4) as functions of stellar parameters. The most important results deduced from our computed W/W^* are an enhancement of NLTE effects with decreasing metallicity, a non monotonic variation with the effective temperature, and a significative dependence on the surface gravity for several lines. We also compare our results with previous works.

4.1 The W/W^* grid for giant and supergiant stars

We compute NLTE/LTE EW ratios for T_{eff} , $\log g$ and $[\text{Fe}/\text{H}]$ covering most of the late-type giant and supergiant stars. The effective temperature T_{eff} range is 3500(200)3900 K and 4000(250)5250 K, the surface gravity $\log g$ range is 0.5(0.5)2.0 dex, and the metallicity $[\text{Fe}/\text{H}]$ range is -4.0(0.5) - 1.00(0.25) + 0.50 dex. We use spherical, 1D, and static model atmospheres from the MARCS site¹⁰ (Gustafsson et al. 2008) with chemical standard composition from Grevesse et al. (2007). In the standard composition of MARCS models, $[\alpha/\text{Fe}]$ depends on $[\text{Fe}/\text{H}]$ as:

$$\begin{aligned}
& [\text{Fe}/\text{H}] \geq 0 \Rightarrow [\alpha/\text{Fe}] = 0 \\
-1 < [\text{Fe}/\text{H}] < 0 \Rightarrow [\alpha/\text{Fe}] = -0.4 [\text{Fe}/\text{H}] \quad (7) \\
& [\text{Fe}/\text{H}] \leq -1 \Rightarrow [\alpha/\text{Fe}] = +0.4
\end{aligned}$$

This means that the Ca abundance used for NLTE computations follows the $[\alpha/\text{Fe}]$ value of the model atmosphere. The MARCS models with $M = 1 M_{\odot}$ and constant microturbulent velocity fields $\xi = 2 \text{ km s}^{-1}$ are adopted. We interpolated MARCS model atmospheres with the Masseron code for $[\text{Fe}/\text{H}] = -3.50$ and for few models missing in the MARCS database.

For the NLTE computations, we need to solve coherently the coupled equations of the SE and the radiative transfer which use the local approximate lambda operator implemented in the 1D, plane-parallel, and time independent code MULTI, version 2.2 (Carlsson 1986). Continuous opacities come from Uppsala package (Gustafsson 1973). We take into account 45000 lines for line opacity computations. Opacities from molecular lines are not included. We

Table 2. Part of the results for the Mg I 8736 Å and Ca II 8498 Å lines. The full version of the results is available in the online version of the journal. NLTE/LTE EW ratios W/W^* are given for $T_{\text{eff}} = 5000 \text{ K}$, $\log g = 1$ and 2, and metallicities if $W > 1 \text{ mÅ}$. We do not take into account collisions with neutral hydrogen ($S_H = 0$). The NLTE abundance correction $\Delta[\text{El}/\text{H}]$ is given when the Eq.(6) is applicable.

$T_{\text{eff}}[\text{K}]$	$\log g$	$[\text{Fe}/\text{H}]$	$[\alpha/\text{Fe}]$	Mg I 8736.012 Å		
				$W[\text{mÅ}]$	W/W^*	$\Delta[\text{Mg}/\text{H}]$
5000	1	+0.50	0.0	225	1.179	
		+0.25	0.0	205	1.226	
		+0.00	0.0	177	1.268	
		-0.25	0.1	158	1.299	
		-0.50	0.2	135	1.302	-0.11
		-0.75	0.3	111	1.272	-0.10
		-1.00	0.4	89	1.210	-0.08
	2	+0.50	0.0	211	1.170	
		+0.25	0.0	192	1.196	
		+0.00	0.0	167	1.214	
		-0.25	0.1	151	1.230	
		-0.50	0.2	131	1.236	-0.09
		-0.75	0.3	110	1.218	-0.09
		-1.00	0.4	88	1.170	-0.07
5000	1	+0.50	0.0	3857	0.969	+0.03
		+0.00	0.0	3086	0.973	+0.02
		-0.50	0.2	2550	0.983	+0.01
		-1.00	0.4	2036	0.993	+0.01
		-2.00	0.4	863	1.037	-0.03
		-3.00	0.4	396	1.154	
		-4.00	0.4	264	1.352	
	2	+0.50	0.0	2255	0.965	+0.03
		+0.00	0.0	1909	0.972	+0.02
		-0.50	0.2	1715	0.984	+0.01
		-1.00	0.4	1446	0.998	+0.00
		-2.00	0.4	737	1.069	-0.06
		-3.00	0.4	370	1.233	
		-4.00	0.4	241	1.435	

do not take into account the collisions with neutral hydrogen ($S_H = 0$). Starting population numbers are taken at LTE and are used to be compared with the NLTE results. With very large model atoms, the convergence of the Newton-Raphson scheme can be very slow and the number of iterations for some extremely metal-poor models can be very high. For the Mg I and Ca II model atoms, the minimal relative precision for the population number at any layer of the atmosphere is of 10^{-4} whereas it decreases to 10^{-3} for Ca I for which the model atom is more complex.

We emphasise that we did 1D NLTE plane-parallel radiative transfer in 1D theoretical spherical model atmospheres which may appear not consistent. However, as shown by Heiter & Eriksson (2006), it is better to use spherical model atmosphere with plane-parallel radiative transfer

¹⁰ available at: <http://marcs.astro.uu.se>

Table 3. Mg I, Ca I and Ca II line selection for NLTE corrections. The wavelengths λ are given in the air. The oscillator strengths gf and the radiative damping parameters γ_{rad} are given in a decimal logarithmic scale. The enhancement factor F_H is defined as the ratio of the collisional damping parameter computed from ABO theory divided by the classical Unsöld's formula (a default value of 2 is applied when lines are outside the range of ABO theory). The radiative damping parameters are calculated using the $\log gf$ values taken from VALD, except when specified. Mg I line selection in the *Gaia*/RVS wavelength range is detailed in Table 4. The precision of $\log gf$ are given with letters, following the NIST notation: A (< 3%), B+ (< 7%), B (< 10%), C+ (< 18%), C (< 25%), D (< 50%), and E (> 50%). Inelastic collisions with electrons are specified in the last column (Coll.) where IPM stands for Impact Parameter Method from Seaton (1962a), CDW stands for Coulomb Distorted Wave approximation from Burgess et al. (1995) for Ca II, and VPM stands for Variable Phase Method from Samson & Berrington (2001) for Ca I resonance lines.

λ [Å]	Lower level			Upper level			$\log gf$	Prec.	$\log \gamma_{\text{rad}}$	F_H	Coll.		
	Configuration	g_i	E_i [eV]	Configuration	g_j	E_j [eV]							
Mg I													
4167.271	3p	$^1P^o$	3	4.345802	7d	1D	5	7.320153	-0.745 ^a	C+	8.71	2.00	IPM
4571.095	4s ²	1S	1	0.000000	3p	$^3P^o$	3	2.711592	-5.688 ^b	C+	2.34	1.34 ^α	IPM
4702.990	3p	$^1P^o$	3	4.345802	5d	1D	5	6.981349	-0.440 ^a	B+	8.72	2.77 ^α	IPM
4730.028	3p	$^1P^o$	3	4.345802	6s	1S	1	6.966284	-2.400 ^b	B+	8.71	2.00	IPM
5167.320	3p	$^3P^o$	1	2.709105	4s	3S	3	5.107827	-0.931 [*]	B	7.98	2.37 ^α	IPM
5172.683	3p	$^3P^o$	3	2.711592	4s	3S	3	5.107827	-0.450 [*]	B	7.98	2.37 ^α	IPM
5183.603	3p	$^3P^o$	5	2.716640	4s	3S	3	5.107827	-0.239 [*]	B	7.98	2.37 ^α	IPM
5528.403	3p	$^1P^o$	3	4.345802	4d	1D	5	6.587855	-0.490 ^b	B+	7.38	2.11 ^α	IPM
5711.086	3p	$^1P^o$	3	4.345802	5s	1S	1	6.516139	-1.720 ^b	B+	8.71	2.00	IPM
7657.599	4s	3S	3	5.107827	5p	$^3P^o$	5	6.726480	-1.268 ^a	C	8.00	2.00	IPM
8473.688	4p	$^3P^o$	5	5.932787	9s	3S	3	7.395551	-2.020 ^c		7.20	2.00	IPM
8806.751	3p	$^1P^o$	3	4.345803	3d	1D	5	5.753246	-0.134 ^a	A	8.72	1.39 ^α	IPM
8923.563	4s	1S	1	5.932370	5p	$^1P^o$	3	7.354590	-1.678 ^a	B	7.81	2.00	IPM
8997.147	4p	$^3P^o$	5	5.932787	8s	3S	3	7.310447	-1.770		7.24	2.00	IPM
10312.52	4p	$^1P^o$	3	5.945915	7d	1D	5	7.364755	-1.730 ^a	C+	8.19	2.00	IPM
11828.18	3p	$^1P^o$	3	4.345802	4s	1S	1	5.753246	-0.333 ^a	A	8.73	2.91 ^α	IPM
Ca I													
4226.727	4s ²	1S	1	0.000000	4p	$^1P^o$	3	2.932512	0.244	B+	8.34	2.09 ^α	VPM
4425.435	4p	$^3P^o$	1	1.879340	4d	3D	3	4.680180	-0.358	C	7.94	1.78 ^α	IPM
4578.549	3d	3D	3	2.521263	4f	$^3F^o$	5	5.228440	-0.697	B+	7.36	2.00	IPM
5512.980	4p	$^1P^o$	3	2.932512	4p ²	1S	1	5.180837	-0.447 ^b	B+	8.48	2.00	IPM
5867.559	4p	$^1P^o$	3	2.932512	6s	1S	1	5.044971	-1.570	B	8.35	2.00	IPM
6102.719	4p	$^3P^o$	1	1.879340	5s	3S	3	3.910399	-0.850 [*]	B	7.87	2.92 ^β	IPM
6122.213	4p	$^3P^o$	3	1.885807	5s	3S	3	3.910399	-0.380 [*]	B	7.87	2.22 ^β	IPM
6161.294	3d	3D	5	2.522986	5p	$^3P^o$	5	4.534736	-1.266	B+	7.30	2.11 ^α	IPM
6162.170	4p	$^3P^o$	5	1.898935	5s	3S	3	3.910399	-0.170 [*]	B	7.87	2.44 ^β	IPM
6166.438	3d	3D	3	2.521263	5p	$^3P^o$	1	4.531335	-1.142	B+	7.28	2.11 ^α	IPM
6169.037	3d	3D	5	2.522986	5p	$^3P^o$	3	4.532211	-0.797	B+	7.30	2.12 ^α	IPM
6169.562	3d	3D	7	2.525682	5p	$^3P^o$	5	4.534736	-0.478	B+	7.30	2.11 ^α	IPM
6455.592	3d	3D	5	2.522986	3d4p	$^1D^o$	5	4.443025	-1.290 ^b	B+	7.67	2.00	IPM
6572.777	4s ²	1S	1	0.000000	4p	$^3P^o$	3	1.885807	-4.296 ^b	D+	3.47	1.57 ^α	VPM
7326.142	4p	$^1P^o$	3	2.932512	4d	1D	5	4.624398	-0.208	B	8.37	1.72 ^α	IPM
8525.707	3d4p	$^3F^o$	5	4.430011	3d5s	3D	3	5.883850	-1.202 ^c		7.70	2.00	IPM
8583.318	3d4p	$^3F^o$	7	4.440954	3d5s	3D	5	5.885035	-0.986 ^c		7.79	2.00	IPM
8633.929	3d4p	$^3F^o$	9	4.450647	3d5s	3D	7	5.886263	-0.810 ^c		7.77	2.00	IPM
Ca II													
3933.663	4s	2P	2	0.000000	4p	$^2P^o$	4	3.150984	0.104 ^b	A+	8.21	1.42 ^α	CDW
3968.468	4s	2P	2	0.000000	4p	$^2P^o$	2	3.123349	-0.210 ^b	A+	8.15	1.43 ^α	CDW
8248.791	5p	$^2P^o$	4	7.514840	5d	2D	6	9.017485	0.556	C	8.29	2.00	IPM
8498.018	3d	2D	4	1.692408	4p	$^2P^o$	4	3.150984	-1.356 ^d		8.21	2.16 ^α	CDW
8542.086	3d	2D	6	1.699932	4p	$^2P^o$	4	3.150984	-0.405 ^d		8.21	2.16 ^α	CDW
8662.135	3d	2D	4	1.692408	4p	$^2P^o$	2	3.123349	-0.668 ^d		8.15	2.16 ^α	CDW
8912.059	4d	2D	4	7.047168	4f	$^2F^o$	6	8.437981	0.575 ^c		8.85	2.00	CDW
9854.752	5p	$^2P^o$	2	7.505137	6s	2S	2	8.762907	-0.260 ^a	D	8.26	2.00	IPM
11949.74	5s	2S	2	6.467874	5p	$^2P^o$	2	7.505137	-0.010	D	8.43	2.00	CDW

^a NIST. ^b Hirata & Horaguchi (1995). ^c Kurucz & Bell (1995). ^d Meléndez et al. (2007). ^{*} Aldenius et al. (2007) for Mg I and Aldenius et al. (2009) for Ca I.

^α ABO theory. ^β Cayrel et al. (1996).

Table 4. Details of the blended multiplets of Mg I in the *Gaia*/RVS wavelengths. The $\log gf$ are from VALD except when specified. The wavelengths in bold and between $\langle \cdot \rangle$ stand respectively for observed lines and Ritz wavelengths (theoretical ones). The notations are the same as in Table 3.

λ [Å]	Lower level Configuration	g_i	E_i [eV]	Upper level Configuration	g_j	E_j [eV]	$\log gf$	Prec.	$\log \gamma_r$	F_H	Coll.
$\langle 8715.255 \rangle$	4p $^3P^o$	9	5.932370	7d 3D	15	7.354590				2.50	IPM
8710.169	4p $^3P^o$	1	5.931542	7d 3D	3	7.354592	-1.565 ^a	D	7.38	2.50	IPM
8712.678	4p $^3P^o$	3	5.931951	7d 3D	8	7.354591	-1.088	D	7.39	2.50	IPM
8712.670		3	5.931951		3	7.354592	-1.690 ^a	D	7.39		
8712.684		3	5.931951		5	7.354590	-1.213 ^a	D+	7.32		
8717.812	4p $^3P^o$	5	5.932787	7d 3D	15	7.354590	-0.866	E	7.39	2.50	IPM
8717.797		5	5.932787		3	7.354592	-2.866 ^a	E	7.38		
8717.811		5	5.932787		5	7.354590	-1.690 ^a	D	7.32		
8717.819		5	5.932787		7	7.354589	-0.941 ^a	D+	7.39		
8736.012	3d 3D	15	5.945915	7f F^o	28	7.364755	-0.351	E	8.21	3.00	IPM
		12	5.945914	$^1F^o$	7	7.364755					
8736.000		5	5.945913		7	7.364755	-3.210 ^c				
8736.014		7	5.945915		7	7.364755	-1.788 ^a	E			
		15	5.945915	$^3F^o$	21	7.364755					
8736.000		5	5.945913		5	7.364755	-1.786 ^a	E			
8736.000		5	5.945913		7	7.364755	-0.890 ^b				
8736.014		7	5.945915		5	7.364755	-3.337 ^a	E			
8736.014		7	5.945915		7	7.364755	-2.170 ^b				
8736.014		7	5.945915		9	7.364755	-0.725 ^a	C			
8736.024		3	5.945917		5	7.364755	-1.056 ^a	D+			

^a NIST. ^b Hirata & Horaguchi (1995). ^c Kurucz & Bell (1995).

rather than plane-parallel model atmosphere with plane-parallel radiative transfer for giant and supergiant stars.

Moreover the W/W^* do not take into account the possible contribution of the stellar chromospheres for lines such as the Mg I b triplet, the Ca II H, K and the Ca T. All the MARCS models are theoretical, 1D and LTE models without any model of chromosphere, i.e. without any rising of the temperature profile in the upper layers. This absence of model chromosphere can explain why we are not able to reproduce the line core of Ca T in Arcturus (Fig. 6). For an extended discussion about the treatment of chromospheric contribution on a peculiar red giant star (β Cet), using this work, see Berio et al. (2011).

The NLTE results for the lines in Tables 3 and 4 are available in electronic forms. Illustrations of W/W^* for a selection of these lines as function of [Fe/H], for several T_{eff} and parametrized in $\log g$ are shown in Appendix A and B. Global NLTE results are summarized in Tables 5, 7 and 8 for Mg I, Ca I and Ca II lines, respectively. We show in Table 2, an example of the NLTE results expressed in terms of W/W^* for the Mg I 8736 Å line and the Ca II IR 8498 Å line as a function of stellar parameters. We also give the NLTE EW in order to know if the Eq. (6) is applicable to directly deduce the NLTE abundance correction $\Delta[\text{E}/\text{H}]$.

4.2 Line selection

The lines are mostly selected as unblended and strong enough to be measurable in metal-poor stars. Spectroscopic and micro-physics details on Mg I, Ca I and Ca II selected lines are presented in Table 3.

Wavelengths are given in air using the IAU standard dispersion law for conversion between vacuum and air (see

Morton 1991). For Mg I, we mainly selected lines of the singlet system except for the Mg I b triplet lines at $\lambda\lambda$ 5167, 5172, 5183, at 7657 and 8997 Å lines, and the lines belonging to the *Gaia*/RVS domain. The important intercombination resonance line at 4571 Å is also selected. This line has been recently studied (Langangen & Carlsson 2009) and has been proposed to be used as temperature diagnostic in stellar atmospheres. For Ca I, we mainly selected lines coming from singly excited levels except for the 5512 Å line and for the weak triplet in RVS because for lines coming from doubly excited levels we have less atomic data. Most of these optical lines are blended in their wings at solar metallicity but are less blended with decreasing metallicity. For the optical red triplet at $\lambda\lambda$ 6102, 6122, 6162, we prefer to use the enhancement factors F_H from Cayrel et al. (1996) who provide resolved F_H for each transition of the triplet ($F_H = 2.92$, 2.22 and 2.44 respectively) rather than ABO theory which gives one unique value of $F_H = 2.55$. Lines selected for Ca II are the strong H & K lines, the IR triplet and few other unblended IR lines.

Lines in the *Gaia*/RVS are dominated by the Ca T. There are also 5 Mg I lines: a very weak line at 8473 Å, a weak triplet at $\lambda\lambda$ 8710, 8712, 8717, and a stronger line at 8736 Å. Details on the components of these lines are shown in Table 4. A partial Grotrian diagram in Fig. 8 also details the fine structure of the levels involved in these multiplets. Note that only the mean level of the 7f $^3F^o$ is available on the NIST database. The weakest 8710 and 8712 Å components of the triplet are also blended on their red wings by iron lines as shown in Fig. 5 and 6. This multiplet at $\lambda\lambda$ 8710, 8712, 8717 is represented, using the Mg I B model, with a Ritz wavelength at 8715 Å for which we deliver NLTE/LTE EW ratio by assuming the same NLTE

Table 5. Mg I W/W^* values for $\log g = 1.5$. Values outside $[0.9, 1.1]$ range are boldfaced. Blanks mean that $W < 1$ mÅ.

$\lambda[\text{\AA}]$	$[\text{Fe}/\text{H}]$ $T_{\text{eff}} [\text{K}]$	-3			-2			0		
		3500	4250	5250	3500	4250	5250	3500	4250	5250
4571.095		0.90	0.34	1.46	0.98	0.69	0.27	0.99	0.97	0.73
4167.271		0.95	0.63	0.57	1.01	0.96	0.85	0.97	0.94	0.97
4702.990		1.18	0.82	0.65	1.08	1.03	0.95	0.97	0.93	0.99
5528.403		1.37	0.96	0.71	1.19	1.11	1.04	0.97	0.92	0.97
8806.751		1.39	1.15	0.91	1.22	1.18	1.24	0.93	0.86	0.95
5167.320		0.95	0.87	0.87	0.91	0.85	0.99	0.93	0.84	0.85
5172.683		0.94	0.82	0.95	0.90	0.83	0.99	0.93	0.83	0.82
5183.603		0.94	0.79	0.97	0.90	0.82	0.97	0.93	0.83	0.81
4730.028		1.39	0.79		1.08	0.94	0.77	0.98	0.92	0.89
5711.086		1.48	0.86		1.22	1.04	0.83	1.01	0.94	0.94
11828.18		1.47	1.23	0.96	1.26	1.24	1.32	0.98	0.87	0.99
8923.563		1.30			1.20		0.68	0.96	0.89	0.86
7657.599 [†]		1.75	0.85		1.48	1.28	0.89	1.12	1.05	0.98
10312.52								0.97	0.95	1.01
8997.147					1.19	1.09		1.02	1.00	1.08
8473.688								1.00	0.97	1.03
$\langle 8715.255 \rangle^{\dagger}$						0.18		1.01	1.10	1.22
8736.012		1.45	0.82		1.08	1.03	0.56	1.36	1.28	1.23

[†] Note that this line is sensitive to the surface gravity.

behaviour for the three components. For Ca I, 5 transitions exist in this domain, between doubled excited levels $3d4p$ and $3d5s$, as shown in Fig. 3. These lines are very weak at solar metallicity and only $\lambda\lambda$ 8525, 8583 and 8633 are visible in the solar spectrum. Moreover, in the spectrum of Arcturus, these three lines are a little bit strengthened but blended by CN lines. Thus, we decide to provide NLTE corrections only for these three lines. We notice that for the $\lambda\lambda$ 8498, 8542, 8662 IR triplet (CaT), we used theoretical $\log gf$ values (-1.356 , -0.405 , -0.668 respectively) from Meléndez et al. (2007) which are in a very good agreement with values derived from 3D hydrodynamical line fits on the Sun (-1.309 , -0.410 , -0.683) from Bigot & Thévenin (2008).

4.3 The Mg I lines

In order to see how the Mg I is affected by the NLTE, the departure coefficients $b_i = n_i/n_i^*$ of the Mg I model atom are plotted in Fig. 7, where n_i and n_i^* stands for NLTE and LTE level populations respectively, as a function of the standard optical depth τ_{5000} for a metal-poor giant model with atmospheric parameters of $T_{\text{eff}} = 4500$ K, $\log g = 2$, $[\text{Fe}/\text{H}] = -3$ and $[\alpha/\text{Fe}] = +0.4$. The ground state is very depopulated regarding the LTE case. This is due to an increase of the UV radiative field produced by a decrease of the metallicity. Moreover, we show that there is an overpopulation of a large part of higher levels explained by a collisional dominated recombination. The population in the ionization stage is in LTE.

The Mg I $\lambda\lambda$ 4167, 4702, 5528 and 8806 lines are transitions between the $3p$ $^1P^o$ level and 1D terms. Therefore, their W/W^* have similar behaviours except for the 8806 Å line which has the most pronounced deviation from LTE (see Table 5 and Fig. A1). At lower metallicities there is a strong variation with T_{eff} and W/W^* can vary between 0.4 and 1.9, which corresponds for weak lines to NLTE abundance cor-

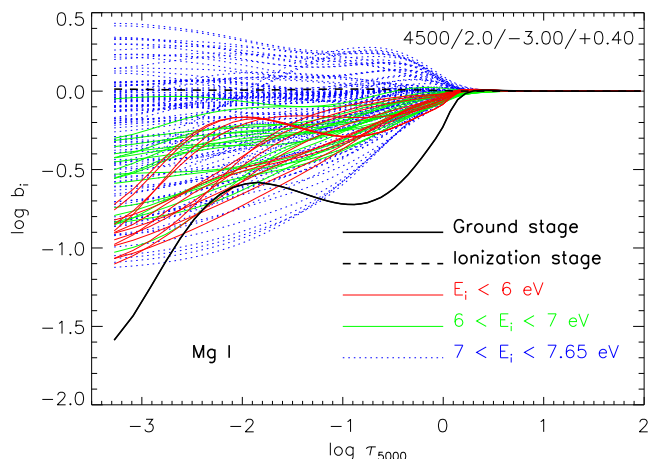


Figure 7. Mg I departure coefficient as a function of optical depth in the continuum at 5000 Å for a metal-poor giant stellar model. We separate levels as function of their energy E_i with respect to the ground state as shown in the legend.

rections between $+0.4$ and -0.3 respectively. Their W/W^* are not sensitive to the surface gravity except for the line at 8806 Å which can have 0.1 dex of difference in abundance correction between $\log g = 1$ and $\log g = 2$ at 4500 K and at solar metallicity.

The Mg I $\lambda\lambda$ 4730, 5711 and 11828 lines also come from the $3p$ $^1P^o$ level and reach 1S terms. The W/W^* of Mg I 4730 and 5711 Å lines have similar trends ($0.9 \leq W/W^* \leq 1.1$ for $-1 \leq [\text{Fe}/\text{H}] \leq +0.5$, stronger NLTE variations otherwise) while the W/W^* of the 11828 Å line is very similar to the W/W^* of the 8806 Å line.

The Mg I 8923 Å line is not very sensitive to the NLTE effects except for models with $T_{\text{eff}} > 4500$ K and $-2 \leq$

Table 6. Comparison of Mg I abundance corrections with Shimanskaya et al. (2000) for five lines as functions of atmospheric parameters. We produce NLTE corrections also taking into account the hydrogen collisions by Drawin’s formula. The Mg abundances of our results follow the enhancement of α -elements of the model atmospheres. Blanks are used when Eq.(6) is not applicable for our NLTE corrections or when W is below 1 mÅ, and when NLTE corrections are not provided by Shimanskaya et al. (2000).

λ [Å]	T_{eff} [K]	$\log g$	4500			5000		
			1			2		
	[Fe/H]		0	-2	-3	0	-2	-3
	NLTE correction	S_H						
4571.095	$\Delta[\text{Mg}/\text{H}]$	0			0.36		0.11	0.48
	$\Delta[\text{Mg}/\text{H}]$	0.1			0.24		0.06	0.26
	$\Delta[\text{Mg}/\text{H}]^\dagger$	0.1	0.03	-0.01	0.14	0.08	0.08	
4702.990	$\Delta[\text{Mg}/\text{H}]$	0	0.05		0.09			0.13
	$\Delta[\text{Mg}/\text{H}]$	0.1	-0.01		0.00			0.00
	$\Delta[\text{Mg}/\text{H}]^\dagger$	0.1	0.01	-0.11	0.02	0.00	0.14	0.14
5183.603	$\Delta[\text{Mg}/\text{H}]$	0	0.20	0.25		0.18		
	$\Delta[\text{Mg}/\text{H}]$	0.1	0.10	0.05		0.10	-0.01	
	$\Delta[\text{Mg}/\text{H}]^\dagger$	0.1		0.02	-0.29		0.00	-0.14
5711.086	$\Delta[\text{Mg}/\text{H}]$	0		-0.01	0.04		0.02	0.10
	$\Delta[\text{Mg}/\text{H}]$	0.1		0.00	0.00		0.00	0.00
	$\Delta[\text{Mg}/\text{H}]^\dagger$	0.1	-0.03	-0.03		-0.03	0.12	
8736.012	$\Delta[\text{Mg}/\text{H}]$	0	-0.11	0.09		-0.09	0.21	
	$\Delta[\text{Mg}/\text{H}]$	0.1	-0.01	0.00		0.00	0.00	
	$\Delta[\text{Mg}/\text{H}]^\dagger$	0.1	-0.05	-0.05		-0.05		

[†] Shimanskaya (private communication)

$[\text{Fe}/\text{H}] \leq -1$ for which we can have $\Delta[\text{Mg}/\text{H}] = +0.15$ dex of abundance correction for the hottest models.

The weak Mg I 10312 Å line is not sensitive to NLTE effects since abundance correction is less than ± 0.05 dex.

The 7657 Å line is the counterpart of the 8923 Å line in the triplet system. This line is in the saturated part of the curve of growth at solar metallicity and becomes weak for $[\text{Fe}/\text{H}] \leq -1$. There is a systematic negative NLTE abundance correction for models with $T_{\text{eff}} \leq 4000$ K that can reach -0.3 dex.

The components of the Mg I b triplet follow the same NLTE trends. When these components are strong with $T_{\text{eff}} \geq 4000$ K and with $-1 \leq [\text{Fe}/\text{H}] \leq +0.5$, the NLTE abundance corrections are positive and vary between $+0.1$ and $+0.3$ dex for the most metal-rich models. For models with $T_{\text{eff}} \geq 4500$ K and with $-4 \leq [\text{Fe}/\text{H}] \leq -3$, strong variations exist for W/W^* that can produce NLTE abundance correction as large as $+0.3$ dex at $[\text{Fe}/\text{H}] = -4$ in the linear regime. The sensitivity of the surface gravity to the NLTE effect is maximum for the intermediate T_{eff} and for the most metal-rich models, and can reach $+0.1$ dex for models between $\log g = 1$ and 2.

We compare our results with those of Shimanskaya et al. (2000) for which grids of stellar parameters overlap. They provided us NLTE corrections for several lines (Shimanskaya, private communication). They take into account inelastic collisions with hydrogen through the use of Drawin’s formula with a scaling factor of $S_H = 0.1$. Therefore, we added hydrogen inelastic collisions with the same scaling factor for six model atmospheres ($T_{\text{eff}} = 4500$ and $\log g = 1$) and ($T_{\text{eff}} = 5000$ K and $\log g = 2$) with $[\text{Fe}/\text{H}] = 0, -2$, and -3 . Results for five lines (λ 4571, 4702, 5183, 5711 and 8736) are presented in Table 6. We formulate three remarks. Firstly, the use of Drawin’s formula reduces strongly

NLTE effects, even with a small scaling factor. Secondly, our NLTE effects are smaller than Shimanskaya et al. (2000) when we use Drawin’s formula. Thirdly, one should be cautious with this comparison because we used different model atoms, model atmospheres, atomic data and codes. We noticed that we have a strong abundance correction for the intercombination resonance 4571 Å line that can reach 0.5 dex even if we treat electronic collision of this line not using the IPM based on the low $\log gf$ value (-5.688), but using a collisional strength Ω_{ij} of 1. Results from Shimanskaya et al. (2000) give lower NLTE abundance correction for this line, maybe because they used isotopic shifts. The 5711 Å line is only affected by NLTE effects at lower metallicities. The subordinate 5183 Å line of the Mg I b triplet is strongly affected by NLTE effects even at solar metallicity with (0.1 dex) and without (0.2 dex) the use of Drawin’s formula.

The Gaia lines

Five Mg I lines from the triplet system belong to the wavelength range of *Gaia*/RVS. These lines are multiplets with poorly known oscillator strengths. The best accuracy for a component of the Mg I 8736 Å line is C (25%) while all the other $\log gf$ have an accuracy of D or E, in the NIST’s definition. In order to deliver NLTE effects for these multiplets, we use the model atom B with merged levels, except for the 8473 Å line. To illustrate the fact that the SE is not disturbed when introducing the merged levels, we compare the level populations of the Mg I model atoms A and B (so the number of levels drops from 150 at 141 in the SE). We compare the sum of populations of fine levels of the Mg I model atom A with the population of the merged levels of the Mg I model atom B. The logarithm of the formed ratio

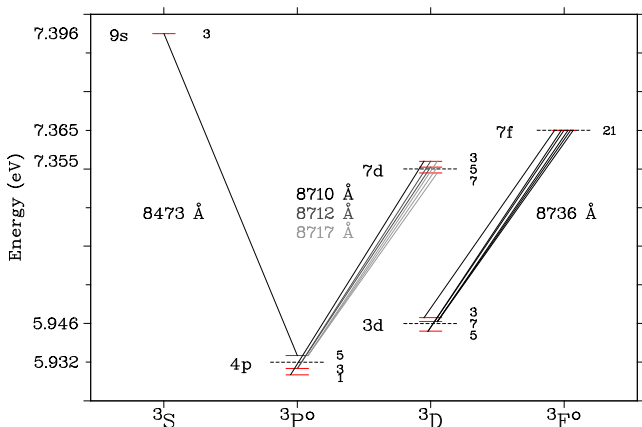


Figure 8. Partial Grotrian diagram for Mg I lines involved in the wavelength domain of *Gaia*/RVS. Mean levels are represented by dashed lines with their NIST values. Statistical weights are represented on the right side of the fine levels.

is plotted for each level considered in Fig. 9. The difference between populations seems to be important, but when we integrate over the depth-scale, the relative error is smaller than 0.1% for $4p\ ^3P^\circ$ and smaller than 0.05% for the three higher levels. We conclude that the merging of fine levels for 4 average levels does not disturb the entire SE of the Mg I atom.

The W/W^* for the Mg I *Gaia*/RVS lines are plotted for several T_{eff} as a function of $[\text{Fe}/\text{H}]$ for each $\log g$ in Fig. B1. The 8473 Å line is the least affected by NLTE effects but vanishes as soon as the metallicity becomes less than -1 dex. The 8715 Å Ritz line (representing a fictitious line with the $\lambda\lambda$ 8710, 8712 and 8717 triplet lines) suffers from large NLTE effects and it is the most sensitive to surface gravity. The NLTE abundance correction can vary of 0.25 dex for $T_{\text{eff}} = 3500$ K, $[\text{Fe}/\text{H}] = -1$ between $\log g = 1$ and 2. The 8736 Å line, which is the most visible Mg I line in this range, disappears under $[\text{Fe}/\text{H}] = -2$. This W/W^* is larger than one for a large range of stellar parameters and can reach 1.4 at solar metallicity.

In our knowledge, there is only NLTE results for the Mg I 8736 Å line in the literature by Shimanskaya et al. (2000). A comparison for six model atmospheres are presented in Table 6. For models at solar metallicity, we are in 0.05 dex agreement. But for the model at $T_{\text{eff}} = 4500$, $\log g = 1$ and $[\text{Fe}/\text{H}] = -2$, we find a positive NLTE abundance correction (for $S_H = 0$). This positive NLTE abundance correction increases with effective temperature and surface gravity whereas this NLTE abundance correction is negative and constant at -0.05 dex for Shimanskaya (private communication). This can be due to the difference in the Mg abundance chosen at this metallicity ($[\text{Mg}/\text{Fe}] = +0.4$ for us versus $+0.00$ for them) and to the value of S_H .

4.4 The Ca I and Ca II lines

4.4.1 The Ca I lines

We show the departure coefficients b_i for the Ca I model atom in Fig. 10, with the same model atmosphere used for the Mg I model atom in Fig. 7, i.e. $T_{\text{eff}} = 4500$, $\log g = 2$ and $[\text{Fe}/\text{H}] = -3$. The ground stage of Ca I is also depopu-

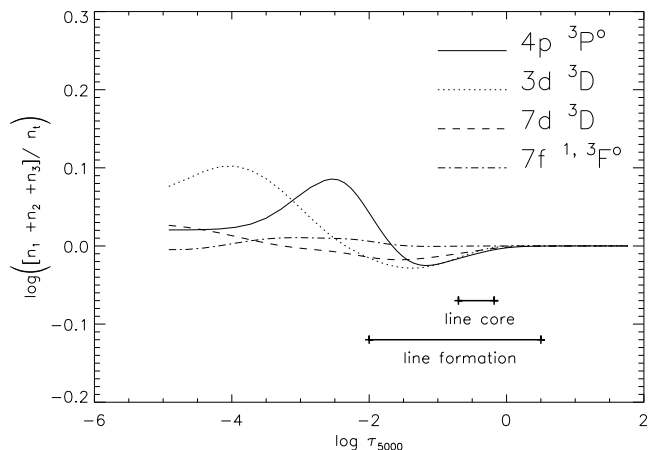


Figure 9. Ratio between sum of detailed level populations ($n_1 + n_2 + n_3$) with average level population (n_t) in logarithmic scale as a function of standard optical depth. For the $7f$ configuration, we merge the terms of the 2 multiplicities. We have represented domain formations of lines in *Gaia*/RVS wavelengths for a solar MARCS model.

lated by overionization but in a lesser extent than for Mg I. In general, the Ca I model is less affected by NLTE effects than the Mg I model for the atmospheric parameters used in this paper. Two mechanisms appear: on the one hand, over-photoionization depopulates lower levels and on the other hand, collisional recombination and photon suction overpopulate levels close to the ionization stage.

The Ca I 4226 Å resonance line shows that its W/W^* is strongly dependent of the three atmospheric parameters (see Table 7 and Fig. A2). For all the models, the NLTE abundance corrections are positive with $\Delta[\text{Ca}/\text{H}] \geq 0.03$. This line is very sensitive to the surface gravity except for $T_{\text{eff}} \geq 5000$ K and $[\text{Fe}/\text{H}] \leq -2$. The NLTE abundance correction can reach $+0.2$ dex between $\log g = 1$ and 2 for the most metal-rich models and $+0.5$ dex for the coolest and most metal-poor models.

The Ca I 6572 Å intercombination and resonance line is also sensitive to the surface gravity but in a lesser extent. This line is weaker than the 4226 Å one and shows that W/W^* depends on the $\log g$ only for models with $T_{\text{eff}} \geq 4000$ K.

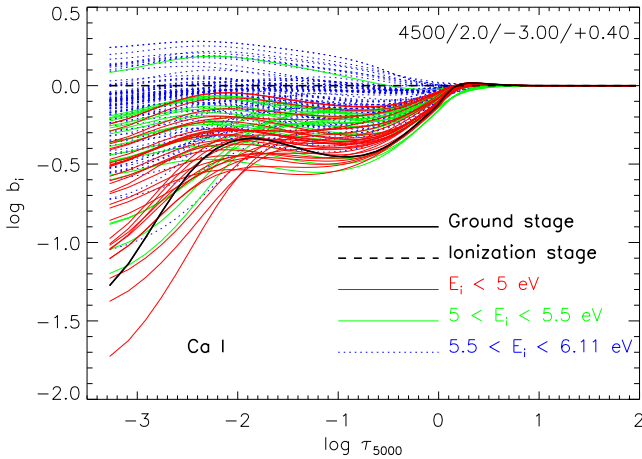
The Ca I $\lambda\lambda$ 5512, 5867 and 7326 lines share the same lower level $4p\ ^1P^\circ$. For these lines, $0.5 \leq W/W^* \leq 1.2$ except for the coolest and most metal-poor model. We can adopt that they are formed under LTE condition in the range of $-1.5 \leq [\text{Fe}/\text{H}] \leq 0$. NLTE abundance correction can be as large as $+0.3$ dex for $[\text{Fe}/\text{H}] \leq -1.5$. For $T_{\text{eff}} < 4000$ K and $[\text{Fe}/\text{H}] < -3$, the 5512 and 7326 Å lines become sensitive to the surface gravity.

For the Ca I red triplet $\lambda\lambda$ 6102, 6122 and 6162 subordinate lines, the NLTE abundance correction are positive for almost all the models. Large deviations from LTE exist for $T_{\text{eff}} < 4500$ K with $-1 \leq [\text{Fe}/\text{H}] \leq +0.5$, and for $T_{\text{eff}} > 4500$ K with $-4 \leq [\text{Fe}/\text{H}] \leq -2.5$. They are not sensitive to the surface gravity.

The Ca I lines at $\lambda\lambda$ 6161, 6166, 6169.0 and 6169.6 belong to the same multiplet. Their W/W^* behaviours are very similar and always less than one, that produces positive NLTE correction. The NLTE abundance corrections can

Table 7. Ca I W/W^* values for $\log g = 1.5$. Values outside $[0.9, 1.1]$ range are boldfaced. Blanks mean that $W < 1 \text{ m}\text{\AA}$.

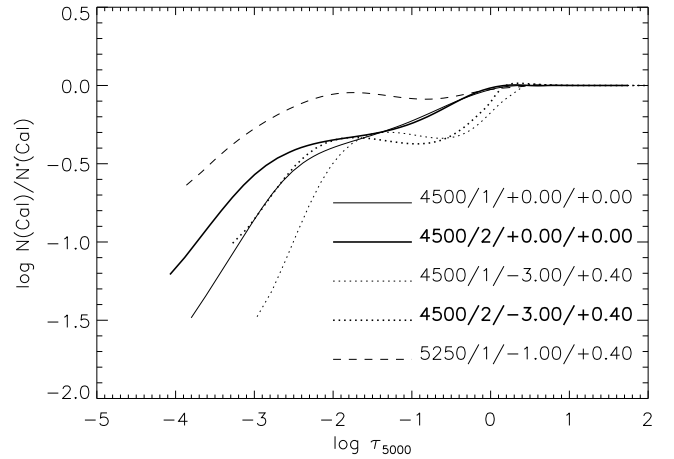
$\lambda[\text{\AA}]$	$[\text{Fe}/\text{H}]$ $T_{\text{eff}} [\text{K}]$	-3			-2			0		
		3500	4250	5250	3500	4250	5250	3500	4250	5250
4226.727 [†]		0.54	0.59	0.93	0.64	0.66	0.86	0.84	0.58	0.81
6572.777 [†]		0.58	0.35		0.85	0.67	0.51	0.93	0.81	0.75
5512.980		1.02	0.61	0.52	1.04	0.92	0.76	0.95	0.97	1.04
5867.559		1.28			1.04	0.92	0.76	0.99	0.87	0.97
7326.142		1.13	0.71	0.51	1.10	1.08	0.85	0.94	0.97	1.08
4425.435		0.83	0.59	0.52	0.85	0.90	0.82	0.81	0.85	0.96
6102.719		0.96	0.64	0.56	0.88	0.99	0.86	0.77	0.83	0.96
6122.213		0.96	0.77	0.60	0.86	1.00	0.97	0.75	0.80	0.98
6162.170		0.92	0.82	0.66	0.84	0.97	1.03	0.74	0.76	0.98
6161.294		0.57	0.40		0.76	0.60	0.58	0.87	0.77	0.83
6166.438		0.55	0.40		0.73	0.60	0.57	0.87	0.78	0.85
6169.037		0.55	0.39	0.39	0.79	0.66	0.57	0.86	0.80	0.88
6169.562		0.59	0.42	0.46	0.83	0.75	0.65	0.84	0.83	0.90
4578.549		0.49	0.36	0.46	0.77	0.65	0.59	0.88	0.87	0.91
6455.592		0.56	0.40		0.77	0.62	0.62	0.92	0.82	0.91
8525.707								0.73	0.60	0.62
8583.318								0.81	0.69	0.73
8633.929								0.88	0.76	0.86

[†] Note that this line is sensitive to the surface gravity.

Figure 10. Ca I departure coefficient as a function of optical depth in the continuum at 5000 Å for a metal-poor giant stellar model ($T_{\text{eff}} = 4500 \text{ K}$, $\log g = 2.0$, $[\text{Fe}/\text{H}] = -3.0$ and $[\alpha/\text{Fe}] = +0.4$). We separate levels as functions of their energy E_i in respect to the ground state as shown in the legend.

reach +0.4 dex for $[\text{Fe}/\text{H}] \leq -3$. These lines are sensitive to the surface gravity for models with $T_{\text{eff}} < 4000 \text{ K}$ and $[\text{Fe}/\text{H}] < -3$.

The line at 4578 Å is also from the same lower term than the previous multiplet. The W/W^* is very similar at low metallicities. We can note that this line is formed in LTE for models with $-1 \leq [\text{Fe}/\text{H}] \leq 0$ (W/W^* between 0.9 and 1).

The Ca I 6455 Å intercombination line also shares the same lower term than the previous multiplet and the 4578 Å line. The W/W^* is also similar and always lower than one. We notice that the lower deviation from LTE comes near to $[\text{Fe}/\text{H}] = -1$.

The Ca I *Gaia*/RVS lines at 8525, 8583 and 8633 Å

Figure 11. Global Ca I departure coefficients for different model atmospheres of $T_{\text{eff}} = 4500 \text{ K}$, $\log g = 1$ (thin lines), $\log g = 2$ (thick lines), and $[\text{Fe}/\text{H}] = 0$ (solid line), $[\text{Fe}/\text{H}] = -3$ (dotted line); and of $T_{\text{eff}} = 5250 \text{ K}$, $\log g = 1$ and $[\text{Fe}/\text{H}] = -1$ (dashed line). The fourth parameter on the plot is the α -enhancement of the model atmosphere.

are strongly affected by NLTE effects at solar metallicity (see Table 7). These lines are weak whatever the stellar parameters (NLTE EW $\sim 50, 70$ and $90 \text{ m}\text{\AA}$ at maximum respectively). The stronger NLTE effects appear for 8525 and 8583 Å lines and can reach $\Delta[\text{Ca}/\text{H}] = +0.4$ dex. For $T_{\text{eff}} > 4250 \text{ K}$ (respectively $T_{\text{eff}} < 4250 \text{ K}$), NLTE effects increase (respectively decrease) with decreasing metallicity as shown in Fig. B1.

We compare our NLTE results with those of Drake (1991) and found opposite effects concerning the variation of overionization with surface gravity. As emphasized in the review of Asplund (2005), Drake unexpectedly found that the over ionization of Ca I decreases with surface gravity

Table 8. Ca II W/W^* values for $\log g = 1.5$. Values outside $[0.9, 1.1]$ range are boldfaced. Blanks mean that $W < 1 \text{ m}\text{\AA}$.

$\lambda[\text{\AA}]$	$[\text{Fe}/\text{H}]$ $T_{\text{eff}} [\text{K}]$	-3			-2			0		
		3500	4250	5250	3500	4250	5250	3500	4250	5250
3933.663		0.97	0.95	0.98	0.96	0.98	0.99	0.99	0.99	0.99
3968.468		0.96	0.95	0.97	0.97	0.98	0.99	0.99	0.99	0.99
8498.018 [†]		1.13	1.06	1.23	1.02	1.00	1.07	0.95	0.94	0.98
8542.086 [†]		1.13	1.02	1.11	1.01	1.00	1.04	0.95	0.95	0.98
8662.135 [†]		1.11	1.02	1.14	1.00	1.00	1.05	0.95	0.95	0.98
8248.791 [‡]				1.12		1.17	1.24	1.13	1.23	1.26
9854.752 [‡]							1.24	1.12	1.22	1.27
8912.059			1.91	1.54		1.55	1.64	1.27	1.37	1.38
11949.74 [†]			1.69	1.57	1.26	1.51	1.80	1.27	1.43	1.51

[†] Note that this line is sensitive to the surface gravity. [‡] Note that this line is sensitive to the surface gravity for the hottest models.

which is explained by an opacity effect that did not convince Asplund (2005). For giant stars, we show in Fig. 11 the opposite effects of overionization, comparing with fig. 6a by Drake (1991). We plot overall Ca I departure coefficient for model atmospheres of $T_{\text{eff}} = 4500 \text{ K}$, $\log g = 1$ and 2, and $[\text{Fe}/\text{H}] = 0$ and -3 . We see that for a given metallicity, the overall Ca I departure coefficient tends to be closer to one with the increase of the surface gravity. This is the opposite of the two models in fig. 6a of Drake ($T_{\text{eff}} = 4500 \text{ K}$, $\log g = 1$ and 0, and $[\text{Fe}/\text{H}] = 0$) where the overionization of Ca I increases when decreasing the surface gravity.

Comparison with the work of Mashonkina et al. (2007) is done even if the grids of stellar parameters do not overlap. They provided NLTE abundance corrections for a grid of dwarfs and subgiants. We compare results for the Sun and for a spherical model at $T_{\text{eff}} = 5000$, $\log g = 3$, $[\text{Fe}/\text{H}] = -2$ and $[\alpha/\text{Fe}] = +0.4$. In order to be the most consistent for the comparison, we use our Ca I/II model atom described in Sect. 2.3.3. Results are shown in Table 9. We found a better agreement with these authors for the metal-poor star rather than for the Sun. Our NLTE abundance corrections for the solar Ca I lines are mainly lower and in opposite sign compared to them. For the metal-poor star, agreement is very satisfactory except for the 4425 Å line for which we have a halved abundance correction. These agreements are found using different geometries for the model atmospheres (plane-parallel Kurucz models for Mashonkina et al. (2007) against spherical MARCS models for us) and different NLTE codes, but give confidence for the NLTE computations done for the grid of late-type giant and supergiant stars.

4.4.2 The Ca II lines

A part of the results for Ca II lines are shown in Table 8 and in Fig. A3. For the strong resonance H & K lines at $\lambda\lambda 3968$ and 3933 respectively, W/W^* is less but close than one except for temperatures below 3900 K. Hence, the NLTE abundance correction does not exceed 0.1 dex between $[\text{Fe}/\text{H}] = +0.5$ and -3 . It can vary between -0.1 and 0.2 dex at the lowest metallicity of -4 dex. We noticed a light sensitivity to the surface gravity for all effective temperatures. For $[\text{Fe}/\text{H}] \leq -2.5$ that can reach 0.1 dex of amplitude between $\log g = 1$ and $\log g = 2$ at 3500 K (see Table 8 and Fig. A3).

The lines at $\lambda\lambda 8248$ and 9854 come from the same

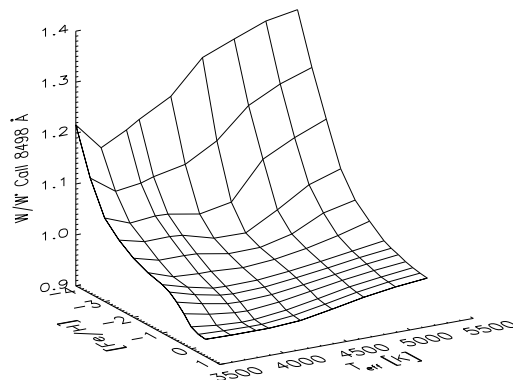


Figure 12. EW ratio of Ca II IR 8498 Å line as a function of effective temperature T_{eff} and metallicity $[\text{Fe}/\text{H}]$, for a given surface gravity $\log g = 1.5$.

$5p^2P^o$ term but from different fine levels and have $W/W^* > 1.1$. The deviation from LTE increases with increasing effective temperature and can reach -0.1 dex of abundance correction. These weak lines are sensitive to the change of the surface gravity for $T_{\text{eff}} \geq 4500 \text{ K}$. These variations can reach 0.05 dex of amplitude between $\log g = 0.5$ and $\log g = 2$.

The NLTE abundance correction for the 8912 Å line can vary between -0.15 dex at solar and subsolar metallicities and -0.3 dex at $[\text{Fe}/\text{H}] = -3.5$ and $T_{\text{eff}} = 4500 \text{ K}$.

The Ca II IR 11949 Å line shows an NLTE sensitivity to the surface gravity (as seen in Fig. A3) that increases with the effective temperature. $W/W^* > 1.2$ for all of the atmospheric parameters.

The NLTE/LTE EW of each component of the CaT follows the same trend. An example of the W/W^* trend of the CaT is shown for the 8498 Å line, which has the most pronounced NLTE effects among the triplet, in Fig. 12 for a surface gravity of $\log g = 1.5$. NLTE effects on the CaT are weak at solar and sub-solar metallicities for all the effective temperatures. For lower metallicities, strong deviations from LTE appear. As shown in Fig. 12, 13 and B2, the W/W^* trends of the CaT as a function of the metallicity can be separated in two regimes:

Table 9. Comparison of Ca I abundance corrections with Mashonkina et al. (2007) for the Sun and for a metal poor sub-giant star without hydrogenic collisions ($S_H = 0$). W represents our NLTE computed EW and W/W^* represents our NLTE/LTE EW ratios. When Eq. (6) is not applicable, blanks are used in $\Delta[\text{Ca}/\text{H}]$ column. Blank in $\Delta[\text{Ca}/\text{H}]^\dagger$ column denotes a NLTE EW less than 5 mÅ.

λ [Å]	Sun				$T_{\text{eff}} = 5000, \log g = 3, [\text{Fe}/\text{H}] = -2$			
	W [mÅ]	W/W^*	$\Delta[\text{Ca}/\text{H}]$	$\Delta[\text{Ca}/\text{H}]^\dagger$	W [mÅ]	W/W^*	$\Delta[\text{Ca}/\text{H}]$	$\Delta[\text{Ca}/\text{H}]^\dagger$
Ca I								
4226.727	1318	0.988	0.01	0.07	543	0.766	0.23	0.24
4425.435	174	1.005		0.04	84	0.830	0.08	0.17
5512.980	96	1.056	-0.01	0.03	20	0.766	0.12	0.10
5867.559	21	1.018	-0.01	0.06	2	0.765	0.12	0.08
6162.170	260	1.037		0.01	128	0.990		0.00
6166.438	65	1.013	-0.01	0.07	9	0.557	0.25	0.30
Ca II								
8248.7907	68	1.184	-0.15	-0.11	5	1.153	-0.06	
8498.0180	1244	1.004	0.00	-0.02	731	1.087	-0.07	-0.08

\dagger Mashonkina et al. (2007)

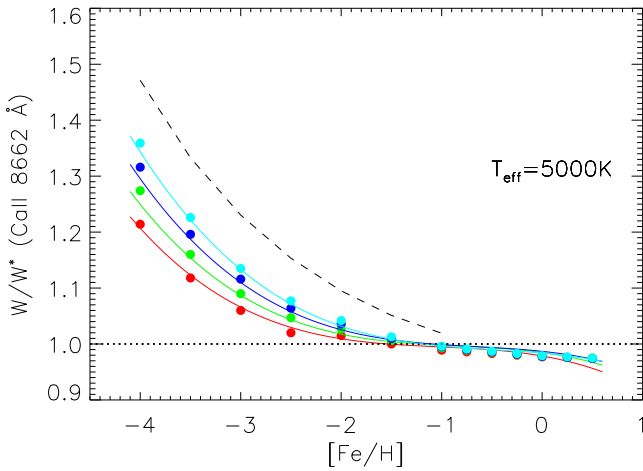


Figure 13. NLTE/LTE EW ratio of Ca II IR 8662 Å line as function of metallicity $[\text{Fe}/\text{H}]$ and $\log g$, for a given effective temperature $T_{\text{eff}} = 5000$ K. Each colour of the W/W^* represents a surface gravity (red, green, blue and cyan for $\log g = 0.5, 1.0, 1.5$ and 2.0 dex respectively). Dots represent computed ratios while full lines represents our polynomial fit of the NLTE/LTE EW ratios. The dashed curve stands for the $W/W^*(8662 \text{ Å})$ polynomial fit computed by Starkenburg et al. (2010).

- the W/W^* is a linear function of the metallicity $[\text{Fe}/\text{H}]$ when $W/W^* \leq 1$;
- the W/W^* increases strongly with decreasing metallicity when $W/W^* > 1$ and can reach 1.45.

Roughly speaking, the CaT lines are formed in LTE ($W/W^* = 1 \pm 0.05$ which corresponds to $\Delta[\text{Ca}/\text{H}] = 0.00 \pm 0.04$ dex) if $-2 \leq [\text{Fe}/\text{H}] \leq 0$ for T_{eff} and $\log g$ in our grid. The CaT lines cannot be considered in LTE when $[\text{Fe}/\text{H}] < -2$, and when $[\text{Fe}/\text{H}] > 0$ for $T_{\text{eff}} < 4000$ K. The NLTE effects decrease with effective temperature and pass through a minimum at ~ 4000 K to increase again at lower T_{eff} , as shown in Fig. 12. This effect may be due to the in-

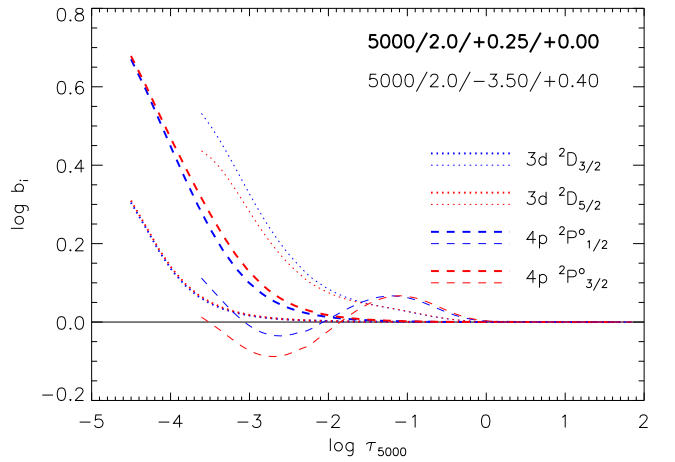


Figure 14. Departure coefficients for fine levels implied in the CaT lines for comparison between a metal rich model atmosphere (bold curves) and an extremely metal poor model (thin curves). The two model atmospheres have $T_{\text{eff}} = 5000$ K and $\log g = 2$, but different global metallicities ($[\text{Fe}/\text{H}] = +0.25$ and -3.5) and different α -enhancement factors ($[\alpha/\text{Fe}] = 0$ and $+0.4$ respectively).

crease of molecular continuous opacities in MARCS models when the effective temperature decreases.

The behaviour of the W/W^* with varying $[\text{Fe}/\text{H}]$ of the CaT can be explained with the variations of the departure coefficients presented in Fig. 14. As the stimulated emission can be neglected for optical and near IR lines, the line source function relative to the Planck function S_ν^l/B_ν follows the departure coefficient ratio b_j/b_i (i and j are the lower and upper levels respectively). The behaviour of the W/W^* depends on the values of b_i relative to b_j and on the deviation between them. In the metal-rich model (in Fig. 14), the levels are over-populated due to overionization of Ca I and $b_i < b_j$ that implies $S_\nu^l > B_\nu$, and the emergent intensity is strengthened in the line compared to LTE intensity. Thus the EW in NLTE is lower than the EW in LTE. This explains why $W/W^* \leq 1$ for models with $-1 \leq [\text{Fe}/\text{H}] \leq +0.5$

Table 10. Comparison of our W/W_J^* with those of Jørgensen et al. (1992) for the same stellar parameters. The NLTE/LTE EW ratio is defined as $W/W_J^* = W(8542\text{\AA} + 8662\text{\AA})/W^*(8542\text{\AA} + 8662\text{\AA})$.

T_{eff} [K]	$\log g$	[Fe/H]	W/W_J^*	$W/W_{J\ddagger}^*$
4000	1	0.00	0.93	0.95
		-0.50	0.95	0.94
		-1.00	0.97	0.95
	2	0.00	0.96	0.97
		-0.50	0.97	0.98
		-1.00	0.98	0.99
5000	1	0.00	0.98	0.99
		-0.50	0.99	0.99
		-1.00	0.99	0.98
	2	0.00	0.98	0.99
		-0.50	0.99	0.99
		-1.00	1.00	0.99

‡ Jørgensen et al. (1992)

in Fig. 13. For the metal-poor model in Fig. 14, the mechanism is the opposite due to the change in the relative values of b_i and b_j . For metallicities lower than -1 , $b_i > b_j$ if $\tau_{5000} \leq -1.7$ and then $S_\nu^l < B_\nu$. This implies a reduction of the emergent intensity in the line and then a larger value of EW in NLTE relative to the LTE. This explains why $W/W^* > 1$ for models with $[\text{Fe}/\text{H}] \leq -1$ in Fig. 13. The large effects at lower metallicity is due to a larger extent of $\log |b_j/b_i|$ compared to solar and sub-solar metallicities.

The fine structure of the levels follows the same trends but level population differences increase with decreasing $\log \tau_{5000}$. The Ca II IR 8498 Å line has the greater NLTE effects relative to the two other lines because it has the largest amplitude on the deviation between the lower coefficient b_i ($3d^2 D_{3/2}$, blue dotted line) and the upper coefficient b_j ($4p^2 P_{3/2}^o$, red dashed line) as seen in Fig. 14. The CaT lines are dominated by their wings even at $[\text{Fe}/\text{H}] = -3$ as shown in fig. 1 of Starkenburg et al. (2010). These wings are formed in the deep photosphere in LTE conditions. Therefore the EW are weakly influenced by NLTE effects at solar metallicity and moderate for most metal-poor stars for which the correction can become very large (20-30% at $[\text{Fe}/\text{H}] = -3$). These results are in quite good agreement with those of previous investigations with the same stellar parameters (e.g. Jørgensen et al. 1992, Andretta et al. 2005).

We note that even if NLTE line formation has almost no influence on Ca abundance determination using the CaT at solar or sub-solar metallicity, it has an impact on the detection of stellar activity. Indeed, the central depression of the CaT is often used as an indicator of activity, (e.g. Andretta et al. 2005, Busà et al. 2007). The detail modelling of the line core formed in NLTE is therefore crucial.

Comparing our results with those of Jørgensen et al. (1992), we find that they are in very good agreement. They combine the two strongest lines of the CaT, noted here W/W_J^* (8542 and 8662 Å) and compute NLTE effects for a large set of gravities (from $\log g = 0.0$ to 4.0) but for a small metallicity range (from -1.0 to 0.2). We give the comparison between our result for the combined lines ratio W/W_J^* in Table 10. Deviation in NLTE effect with these authors are less than 2%. The NLTE EW increases with increasing metallicity ($-1 < [\text{Fe}/\text{H}] < +0.25$) but our EW are

larger by a factor of 2 with those of Jørgensen et al. ones at $[\text{Fe}/\text{H}] = -1$. This may come from the fact that their model atmospheres are not α -enhanced at lower metallicities. Note also that they do not have the photoionization cross-sections from the TopBase and ABO theory. Other authors computed NLTE effects for the CaT but for late-type dwarf stars (e.g. Andretta et al. 2005). They found values of W/W^* always larger than 1 reaching 1.35 at lower metallicity ($[\text{Fe}/\text{H}] = -2$).

We also compared the NLTE effects on CaT computed by Starkenburg et al. (2010) and found a clear discrepancy at low metallicity. They provided a 2D polynomial fit of $W^*/W = f(T_{\text{eff}}, [\text{Fe}/\text{H}])$ for the lines at 8542 Å and 8662 Å, considering that these ratios are insensitive to the surface gravity ($1 \leq \log g \leq 2$). We plotted in Fig. 13 and A3 their polynomial fit for the 8662 Å line. The discrepancies between our W/W^* and theirs, at a given T_{eff} , increase with decreasing metallicity and with decreasing surface gravity. At $[\text{Fe}/\text{H}] = -4$, the deviation is about 10% for $\log g = 2$ and about 18% for $\log g = 1$. These differences may come from the fact that they used a different geometry (plane-parallel) in their study. We checked that the use of the scaling factor $S_H = 1$ for the collisions with neutral hydrogen cannot compensate this difference. Note that they not clearly indicate the value of Ca abundance that they used for the computations of the W/W^* .

Since Starkenburg et al. (2010) used the model atom of Mashonkina et al. (2007), we investigate the effects of the different atomic physics injected in the two model atoms of Ca I/II. We consider a stellar model ($T_{\text{eff}} = 5000$ K, $\log g = 3$, $[\text{Fe}/\text{H}] = -2$), which is outside of our grid, but used in Mashonkina et al. (2007) to compare with. Our predictions for the two Ca II lines (8248 and 8498 Å) in this particular case are shown in Table 9. We note a difference of 0.04 dex for the weak line at 8248 Å for the Sun and a very good agreement (better than 0.01 dex) for the Ca II IR 8498 Å line for the metal-poor model atmosphere. Therefore, the discrepancy with Starkenburg et al. (2010) does not come from the model atoms. It must be investigated in more details since the calibration between the CaT and $[\text{Fe}/\text{H}]$, as defined in their paper, may be affected for RGB metal-poor stars.

Interesting opposite NLTE trends appear between Ca I and Ca II lines. In general, W/W^* for Ca I lines are smaller than 1.0, whereas W/W^* for Ca II lines are larger than 1.0, whatever the stellar parameters. We note that the NLTE effects are anti-correlated between the Ca I $\lambda\lambda$ 6102, 6122, 6162 triplet lines and the CaT lines in metal-poor model atmospheres. This may have a large impact on the Ca abundance analysis in metal-poor red giants; such remark has already been mentioned in the *Gaia* context (Recio-Blanco & Thévenin 2005).

4.5 Uncertainty estimations

Uncertainties of W/W^* rely on the atomic parameters and on the assumptions of the stellar atmosphere modelling (viz 1D, static, NLTE radiative plane parallel transfer with MULTI code using 1D, static, LTE, spherical MARCS model atmospheres). We computed W/W^* varying atomic parameters in order to estimate uncertainties of the input atomic physics. We selected four model atmospheres ($T_{\text{eff}} = 5000$ K,

Table 11. Fit coefficients of NLTE/LTE EW ratio $[W/W^*]_{\text{fit}}$ for lines in the *Gaia*/RVS wavelength range. The fits are valid for $3500 \leq T_{\text{eff}} \leq 5500$ K, $0.5 \leq \log g \leq 2$ and $[\text{Fe}/\text{H}]_{\text{min}} \leq [\text{Fe}/\text{H}] \leq +0.5$. The Mg and Ca abundances follow the α -enhancement given in Eq. (7). The blanks denote coefficients related to discarded terms. ϵ_{max} and ϵ_{mean} are given (in %) as the maximum and the mean absolute difference between $[W/W^*]_{\text{fit}}$ and W/W^* .

λ [Å]	Mg I			Ca I			Ca II		
	8473.688	(8715.255)	8736.012	8525.707	8583.318	8633.929	8498.018	8542.086	8662.135
$[\text{Fe}/\text{H}]_{\text{min}}$	-1.0	-1.5	-2.0	-1.0	-1.0	-1.0	-4.0	-4.0	-4.0
a_0	1.03E+0	1.22E+0	1.31E+0	5.95E-1	7.05E-1	7.97E-1	9.88E-1	9.72E-1	9.73E-1
a_1	3.32E-2	1.43E-1	-6.84E-2	-2.81E-2		6.00E-2	3.68E-2	3.71E-2	3.82E-2
a_2	-1.79E-2	-9.26E-2	-2.36E-2	-1.67E-2			9.15E-3	3.05E-3	2.21E-3
a_3	-1.48E-1	-3.90E-2	1.61E-1	7.11E-2	2.76E-2		-8.44E-2	-2.74E-2	-3.18E-2
a_4	1.50E-2	-1.04E-1	-6.34E-2	4.74E-2	5.13E-2	6.63E-2	4.22E-2	4.66E-2	4.60E-2
a_5		6.79E-2		2.41E-2	2.12E-2	2.02E-2			
a_6		-2.76E-2		1.22E-2				6.45E-3	
a_7	2.24E-2	-1.86E-2	8.05E-2	2.09E-1	1.84E-1	1.32E-1	-3.87E-2	5.33E-3	-1.67E-2
a_8	4.39E-2	9.46E-2	-2.16E-2	5.01E-2	3.87E-2	2.81E-2	-3.81E-2	-2.93E-2	-2.91E-2
a_9		-2.95E-1	-2.42E-1	-2.49E-2	-3.69E-2	-3.44E-2	1.12E-1	7.77E-2	9.38E-2
a_{10}	-2.31E-2		3.44E-2	-9.98E-2	-1.02E-1	-1.20E-1	-2.54E-2	-2.43E-2	-2.32E-2
a_{11}	-6.92E-3	-2.49E-2	-2.50E-2	1.61E-2			1.15E-2	1.42E-2	1.34E-2
a_{12}								-1.08E-2	-9.03E-3
a_{13}									
a_{14}	4.43E-2	1.84E-1	1.20E-1				-3.22E-2	-5.32E-2	-5.47E-2
a_{15}	-1.23E-2	-6.67E-2							
a_{16}		2.82E-2						-5.81E-3	
a_{17}	-2.26E-2	-7.15E-2	-1.18E-1	1.04E-2	1.14E-2	1.53E-2	4.17E-2		2.07E-2
a_{18}	1.90E-2		5.08E-2	1.06E-2	6.51E-3		2.93E-2	2.95E-2	3.21E-2
a_{19}	3.75E-2	1.72E-1	-5.34E-2	6.04E-2	6.25E-2	4.85E-2	-7.47E-2	-7.74E-2	-8.14E-2
ϵ_{max}	3.4	7.0	9.3	4.7	4.5	4.6	6.0	7.2	8.3
ϵ_{mean}	0.7	1.6	2.2	1.4	1.4	1.2	0.9	1.0	1.0
$\epsilon_{\text{max}}^{\dagger}$							2.3	4.6	4.2
$\epsilon_{\text{mean}}^{\dagger}$							0.6	0.8	0.8

\dagger if $[\text{Fe}/\text{H}] \geq -2$

$\log g = 2$, $[\text{Fe}/\text{H}] = 0, -2$; and $T_{\text{eff}} = 4500$ K, $\log g = 1$, $[\text{Fe}/\text{H}] = 0, -2$ and three lines (one resonance, one subordinate, and one allowed lines) for each model atom ($\lambda\lambda$ 4571, 5183, 8806 for Mg I, $\lambda\lambda$ 6162, 6166, 6572 for Ca I, and $\lambda\lambda$ 3933, 8248, 8498 for Ca II). The Mg I 4571 Å and the Ca I 6572 Å lines are the equivalent intercombination resonance lines for Mg I and Ca I model atoms. For each line, the uncertainties of three atomic parameters were tested: the oscillator strengths, the photoionization cross-sections and the effective collisional strengths with electrons. We emphasize that we performed these uncertainty estimations over a hundred of runs (3 among 45 lines over 4 among 453 model atmospheres) to give a rough idea of the impact of the uncertainties on atomic data.

We tested for each model atoms the change of the oscillator strengths of the three lines by $\pm 50\%$. The changes on the W/W^* for the three lines are less than 8%. For instance, with the model at $T_{\text{eff}} = 5000$ K, $\log g = 2$, $[\text{Fe}/\text{H}] = -2$, we obtained $W/W^*(\text{Mg I } 8806 \text{ \AA}) = 1.35_{-0.06}^{+0.02}$, $W/W^*(\text{Ca I } 6572 \text{ \AA}) = 0.53_{-0.02}^{+0.01}$ and $W/W^*(\text{Ca II } 8498 \text{ \AA}) = 1.07_{-0.02}^{+0.03}$. We remind that the accuracy of the $\log gf$ used and given in Table 3 and 4 varies between 2% and 50%. Therefore, these uncertainties can be seen as an upper limit. We noticed that the W/W^* are more affected by changes of oscillator strength values for the metal-poor model atmospheres.

Varying the amplitudes of the photoionization cross-sections does not affect the lines of model atoms in the same

way. We changed by a factor ± 2 the amplitude of the Top-Base photoionization cross-sections of the lower levels of the lines considered. The Mg I model atom is the most affected with variations on the W/W^* that can reach +8% (for instance $W/W^*(\text{Mg I } 5183 \text{ \AA}) = 0.79_{-0.03}^{+0.03}$ for the model with $T_{\text{eff}} = 4500$ K, $\log g = 1$, $[\text{Fe}/\text{H}] = 0$). Calcium is less affected, with 1% of variations of W/W^* for the Ca I and less than 1% for the Ca II model atoms. As emphasized by Mashonkina et al. (2007), the changes of the photoionization cross-sections mainly affect the minority species (Ca I in the range of stellar parameters considered here). However, we found that the absolute corrections on the W/W^* increase with decreasing metallicity, due to variations on the amplitude of photoionization cross-sections.

Finally, we tested the variations of the amplitude of the collisional strength with electrons. Using the IPM approximation, the change by a factor of ± 2 of the effective collisional strength slightly affects the W/W^* results (less than $\leq 2\%$).

4.6 Polynomial fit of the W/W^* for the *Gaia* lines

Due to the importance of the Ca I and the Mg I 8736 Å for the *Gaia*/RVS mission, we provide a fit of the W/W^* presented in the previous section as a multivariable polynomial for the five Mg I lines, the three Ca I lines and the Ca I lines. The expression of the fit is up to the third order in stellar parameters:

$$\left[\frac{W}{W^*} \right]_{\text{fit}}(x, y, z) = \quad (8)$$

$$\begin{aligned} & a_0 & + & a_1 x & + & a_2 y & + & a_3 z \\ + & a_4 x^2 & + & a_5 xy & + & a_6 y^2 & + & a_7 xz \\ + & a_8 yz & + & a_9 z^2 & + & a_{10} x^3 & + & a_{11} x^2y \\ + & a_{12} xy^2 & + & a_{13} y^3 & + & a_{14} x^2z & + & a_{15} xyz \\ + & a_{16} y^2z & + & a_{17} xz^2 & + & a_{18} yz^2 & + & a_{19} z^3 \end{aligned}$$

with:

$$\begin{aligned} x &= (T_{\text{eff}} - 4375)/875 \\ y &= (\log g - 1.25)/0.75 \\ z &= ([\text{Fe}/\text{H}] - [\text{Fe}/\text{H}]_c)/(0.5\Delta[\text{Fe}/\text{H}]) \end{aligned} \quad (9)$$

the reduced and centred variables that lead to a variation in the $[-1, 1]$ range for our ranges of atmospheric parameters. $\Delta[\text{Fe}/\text{H}]$ represents the metallicity range and $[\text{Fe}/\text{H}]_c$ is the median metallicity, which depends on the line considered. As $[\text{Fe}/\text{H}]_{\text{max}} = +0.50$ in all cases, the median metallicity and the metallicity range are expressed by:

$$[\text{Fe}/\text{H}]_c = \frac{1}{2}[\text{Fe}/\text{H}]_{\text{min}} + 0.25$$

$$\Delta[\text{Fe}/\text{H}] = [\text{Fe}/\text{H}]_{\text{max}} - [\text{Fe}/\text{H}]_{\text{min}}$$

where $[\text{Fe}/\text{H}]_{\text{min}}$ is specified in the Table 11. As seen in Figs. B1 and B2, the NLTE/LTE EW ratios have different behaviours in stellar parameters for each line considered. A second order formula (Andretta et al. 2005) or modified second order (Starkenburger et al. 2010) is not enough to fit the dependence, especially for $[\text{Fe}/\text{H}]$ at low metallicity (≤ -3). In order to find the coefficients a_m ($m = 0, 19$), we use the LSQ package of Miller (1992) and we rejected W/W^* values for which $W < 1 \text{ m}\text{\AA}$. We present the results in Table 11 for the Mg I, Ca I and Ca II *Gaia*/RVS lines. We noticed that some terms may be discarded without modifying the accuracy of the fit: the related coefficients are represented by blanks in Table 11. For instance, we see that for Mg I and Ca I lines, the fits are insensitive to the xy^2 and y^3 terms; for the Ca T, the fits are insensitive to the xy , y^3 and xyz terms.

Examples of the fits are shown in Fig. 13 for the Ca II IR 8662 Å and in Figs. B1 and B2 for the other *Gaia*/RVS lines. For the *Gaia*/RVS Mg I and Ca I lines we restrict the range of metallicities as indicated in Table 11 since below the lower metallicities the line is too weak ($W \leq 1 \text{ m}\text{\AA}$) to be considered. These fits can be used to estimate the NLTE/LTE EW ratios with an accuracy better than 10%, in the range of the stellar parameters considered. The largest deviations of the fits appear for the most metal-poor model atmospheres for the Mg I 8736 Å and the Ca T lines. Hence, when requested accuracy is greater than ϵ_{mean} (given in % in Table 11), our fits can be used with confidence. Otherwise, it is advised to directly use W/W^* in the electronic tables.

5 CONCLUSION

We have performed NLTE computations for the Mg I, Ca I and Ca II model atoms in late-type giant and supergiant stars. We provide NLTE/LTE EW ratios for a grid of 453 MARCS model atmospheres ($3500 \leq T_{\text{eff}} \leq 5250 \text{ K}$, $0.5 \leq \log g \leq 2.0 \text{ dex}$ and $-4.00 \leq [\text{Fe}/\text{H}] \leq +0.50 \text{ dex}$)

in electronic forms¹¹. The model atoms are based on the assumption that we do not take into account inelastic collisions with neutral hydrogen since realistic quantum mechanical collisional cross-sections are still unavailable. We used a formulation for electronic collisions that underestimate the collisional rate. Such underestimation induced an upper limit on the NLTE/LTE EW ratios especially for the Mg I lines in the *Gaia*/RVS wavelength range. The use of fine structure in the model atoms do not affect strongly NLTE results since the W/W^* of the components of a multiplet are very similar but permit a consistent representation of the physics. This work will be extended to late-type main sequence stars when collisional cross-sections with hydrogen are available.

The main conclusions for the lines outside the *Gaia*/RVS wavelength range are as follows. For the Mg I and Ca I lines, the assumption of LTE underestimates the Mg and the Ca abundances and gives mainly positive NLTE abundance correction. For the Ca II lines, the assumption of LTE overestimates the Ca abundance and gives mainly negative NLTE abundance corrections. However, most of the Mg I lines show $W/W^* > 1$ that can reach 2 for the coolest models with an increase of the sensitivity to the surface gravities. The Mg I b and Ca I red triplets show $W/W^* < 1$ that can reach 0.5 for the most metal-poor and the hottest model atmospheres. The NLTE effects for the Mg I 4571 Å and the Ca I 6572 Å intercombination and resonance lines are very sensitive to the metallicity and to the surface gravity. The NLTE effects on Ca II H&K lines are negligible except at $[\text{Fe}/\text{H}] = -4$.

For the *Gaia*/RVS lines, NLTE computations give the following trends. The very weak 8473 Å line is mainly formed in LTE whereas the Mg I 8736 Å and the Mg I $\lambda\lambda$ 8710, 8712 and 8717 triplet lines are mainly formed in NLTE with a strong sensitivity to the surface gravity for the triplet. The weak Ca I triplet lines are mainly formed in NLTE but vanish as soon as $[\text{Fe}/\text{H}] < 1$. The famous Ca T lines are mainly formed in LTE if $[\text{Fe}/\text{H}] \geq -2$. The NLTE effects increase with a decrease of the metallicity and with an increase of the surface gravity. We show that the $W/W^*(\text{Ca T})$ can increase by 20% for $\log g$ varying from 0.5 to 2.0. For convenience, we provide a polynomial fit computed for the *Gaia*/RVS lines: the Mg I $\lambda\lambda$ 8473, (8715) triplet, 8736 multiplet, the Ca I $\lambda\lambda$ 8525, 8583 and 8633, and the Ca T lines. The polynomial can be extensively used by the automatic tools dedicated to the analysis and extract chemical abundances for millions of stars in the context of the large surveys as, for example, *Gaia* and RAVE.

ACKNOWLEDGMENTS

TM is granted by OCA and Région PACA, and supported by Thalès Alenia Space. This work was supported by the "Action Spécifique Gaia". Part of computations were performed with the "Mesocentre SIGAMM" machine, hosted by the Observatoire de la Côte d'Azur. The authors acknowledge the role of the SAM collaboration (<http://www.anst.uu.se/ulhei450/GaiaSAM>) in stimulating

¹¹ available on the Vizier/CDS database

this research through regular workshops. TM also thanks J. Tully and M. Carlsson for helpful discussions.

REFERENCES

- Aldenius M., Lundberg H., Blackwell-Whitehead R., 2009, *A&A*, 502, 989
- Aldenius M., Tanner J. D., Johansson S., Lundberg H., Ryan S. G., 2007, *A&A*, 461, 767
- Allen C. W., 1973 *Astrophysical Quantities*, 3rd Edition, Athlone Press, London
- Andretta V., Busà I., Gomez M. T., Terranegra L., 2005, *A&A*, 430, 669
- Andrievsky S. M., Spite M., Korotin S. A., Spite F., Bonifacio P., Cayrel R., François P., Hill V., 2010, *A&A*, 509, 88
- Anstee S. D., O'Mara B. J., 1995, *MNRAS*, 276, 859
- Asplund M., 2005, *ARA&A*, 43, 481
- Asplund M., Grevesse N., Sauval J., Scott P., 2009, *ARA&A*, 47, 481
- Ayres T. R., Simon T., Linsky J. L., 1982, *ApJ*, 263, 791
- Barklem P. S., O'Mara B. J., 1997, *MNRAS*, 290, 102
- Barklem P. S., O'Mara B. J., 1998, *MNRAS*, 300, 863
- Barklem P. S., Belyaev A. K., Asplund M., 2003, *A&A*, 409, L1
- Barklem P. S., Belyaev A. K., Guitou, M., Feautrier, N., Gadea, F. X., Spielfiedel, A., 2011, under press, arXiv:1104.1334
- Barklem P. S., O'Mara B. J., Ross J. E., 1998, *MNRAS*, 296, 1057
- Berio P., Merle T., Thévenin F. et al., 2011, *A&A* submitted
- Bigot L., Thévenin F., 2008, SF2A-Proceedings of the Annual meeting of the French Society of Astronomy and Astrophysics Eds.: C. Charbonnel et al., p 3
- Brault J., Neckel H. 1987, Spectral atlas of solar absolute disc-averaged and disc-center intensity from 3290 to 12510Å, unpublished
- Burgess A., Chidichimo M. C., Tully J. A., 1995, *A&A*, 300, 627
- Butler K., Giddings J, 1985, Newsletter on the Analysis of Astronomical Spectra No. 9, University of London
- Busà I., Aznar Cuadrado R., Terranegra L., Andretta V., Gomez M. T., 2007, *A&A*, 466, 1089
- Caccin B., Gomez M. T., Severino G., 1993, *A&A*, 276, 219
- Carlsson M., 1986, A Computer Program for Solving Multi-Level Non-LTE Radiative Transfer Problems in Moving or Static Atmospheres, Report No. 33, Uppsala Astronomical Observatory
- Carlsson M., Rutten R. J., Shchukina N. G., 1992, *A&A*, 253, 561
- Cayrel R., Depagne E., Spite M., Hill V., Spite F., François P., Plez B., Beers T., Primas F., Andersen J., Barbuy B., Bonifacio P., Molaro P., Nordström B., 2004, *A&A*, 416, 1117
- Cayrel R., Faurobert-Scholl M., Feautrier N., Spielfiedel A., Thévenin F., 1996, *A&A*, 312, 549
- Chang E. S., Noyes R. W., 1983, *ApJ*, 275, L11
- Christlieb N., Bessell M. S., Beers T. C., Gustafsson B., Korn A., Barklem P. S., Karlsson T., Mizuno-Wiedner M., Rossi S., 2002, *Nature*, 419, 904
- Cunto W., & Mendoza C., 1992, *Rev. Mex. Astron. Astrofis.*, 23
- De Silva G. M., Freeman K. C., Bland-Hawthorn J., Asplund M., Williams M., Holmberg J., 2011, *MNRAS*, under press, arXiv:1103.2588
- Drake J. J., 1991, *MNRAS*, 251, 369
- Drawin H. W. 1968, *Z. Phys.*, 211, 404
- Edvardsson B., Andersen J., Gustafsson B., Lambert D. L., Nissen P. E., Tomkin J., 1993, *A&A*, 274, 101
- Gehren T., Shi J. R., Zhang H. W., Zhao G., Korn A. J., 2006, *A&A*, 451, 1065
- Gratton R. G., Carretta K., Eriksson K., Gustafsson B., 1999, *A&A*, 350, 955
- Green L. C., Rush P. P., Chandler C. D., 1957, *ApJS*, 3, 37
- Grevesse N., Asplund M., Sauval A. J., 2007, *Space Sci Rev*, 130, 105
- Guitou M., Belyaev A.K., Barklem P.S., Spielfiedel A., Feautrier N., 2010, *J. Phys. B*, under press
- Gustafsson B., 1973, *Uppsala Astr. Obs. Ann.*, 5, No. 6
- Gustafsson B., Edvardsson B., Eriksson K., Jørgensen U. G., Nordlund Å, Plez B., 2008, *A&A*, 486, 951
- Heiter U., Eriksson K., 2006, *A&A*, 452, 1039
- Hirata R., Horaguchi T., 1995, *Catalogue of Atomic Spectroscopic Lines*, Vol. 6 (Strasbourg : CDS), 69
- Idiart T, Thévenin F., de Freitas Pacheco J. A., 1997, *AJ*, 113, 1066
- Idiart T, Thévenin F., 2000, *ApJ*, 541, 207
- Jørgensen U. G., Carlsson M., Johnson H. R., 1992, *A&A*, 254, 258
- Karzas W. J., Latter R., 1961, *Phys. Rev. A*, 13, 1416
- Katz D., et al., 2004, *MNRAS*, 354, 1223
- Kupka F., Ryabchikova T. A., Piskunov N. E., Stempels H.C., Weiss W.W., 2000, *Baltic Astronomy*, vol. 9, 590-594
- Kurucz R. L., Bell B., 1995, *Atomic Line Data Kurucz CD-ROM No. 23*. Cambridge.
- Kurucz R. L., 2005, *MSAIS*, 8, 76
- Langangen Ø., Carlsson M., 2009, *ApJ*, 696, 1892
- Leenaarts J., Carlsson M., Hansteen V., Rouppe van der Voort L., 2009, *ApJ*, 694, L128
- Liu Y., Sato B., Takeda Y., Ando H., Zhao G., 2010, *PASJ*, 62, 1071
- Mashonkina L. I., Korn A. J., Przybilla N., 2007, *A&A*, 461, 261
- Mashonkina L. I., Shimanskaya N. N., Sakhbullin N. A., 1996, *Astron. Reports*, 40, 187
- Meléndez M., Bautista M. A., Badnell N. R., 2007, *A&A*, 469, 1203
- Butler K., Mendoza C., Zeippen C. J., 1993, *J. Phys. B*, 26, 4409
- Menzel D. H., Pekeris C. L., 1935, *MNRAS*, 96, 77
- Mihalas D., 1978, *Stellar atmospheres 2nd Edition*, San Francisco.
- Miller A. J., 1992, *Algorithm AS 274:Least squares routines to supplement those of Gentleman*, *Appl. Statist.*, 41, 458
- Mishenina T. V., Soubiran C., Kovtyukh V. V., Korotin S. A., 2004, *A&A*, 418, 551
- Morton D. C., 1991, *ApJS*, 77, 119
- Nakamura T., Umeda H., Nomoto K., Thielmann F.-K., Burrows A., 1999, *ApJ*, 517, 193
- Przybilla N., Butler K., Becker S.R., Kudritzki R. P., 2001,

A&A, 369,1009

- Recio-Blanco A., Thévenin F., 2005, Proceedings of the Gaia Symposium "The Three-Dimensional Universe with Gaia" (ESA SP-576). Observatoire de Paris-Meudon, 4-7 October 2004. Editors: C. Turon, K.S. O'Flaherty, M.A.C. Perryman.
- Ralchenko Yu., Kramida A. E., Reader J., and NIST ASD Team (2008). NIST Atomic Spectra Database (version 3.1.5), [Online]. Available: <http://physics.nist.gov/asd3> [2010, January 20]. National Institute of Standards and Technology, Gaithersburg, MD.
- Samson A. M., Berrington K. A. 2001, ADNDT,77, 87
- Saraph H. E., Storey, P. J., unpublished
- Seaton M. J., 1962a, Proc. Phys. Soc. London, 79, 1105
- Seaton M. J., 1962b, *Atomic and Molecular Processes* ed. D. R. Bates (New York: Academic Press), 375
- Seaton, M. J.; Yan, Y.; Mihalas, D.; Pradhan, A. K, 1994, MNRAS, 266, 805
- Shimanskaya N. N., Mashonkina L. I., Sakhibullin N. A., 2000, ARep, 44, 530
- Starkenbug E., Hill V., Tolstoy E., González Hernández J. I., Irwin M., Helmi A., Battaglia G., Jablonka P., Tafelmeyer M., Shetrone M., Venn K., de Boer T., 2010, A&A 513, 34
- Steinmetz, M., Zwitter, T., Siebert, A., et al. 2006, AJ, 132, 1645
- Sundqvist J. O., Ryde N., Harper G. M., Kruger A., Richter M. J., 2008, A&A, 486, 985
- Thévenin F., 1989, A&AS, 77, 137
- Thévenin F., 1998, VizieR On-line Data Catalog: III/193
- Thévenin F., Idiart T., 1999, ApJ, 521, 753
- Unsöld A., 1955, *Physik der Sternatmosphären* (Berlin, Springer)
- Vernazza J. E., Avrett E. H., Loeser R., 1981, ApJS, 45, 635
- Wilkinson M. I. et al., 2005, MNRAS, 359, 1306
- Zhao G., Butler K., Gehren T., 1998, A&A, 333, 219
- Zhao G., Gehren T., 2000, A&A, 362, 1077

APPENDIX A: W/W^* FOR THE LINES OUTSIDE OF THE GAIA/RVS WAVELENGTH RANGE

We present the results of the NLTE computations as the evolution of the NLTE/LTE EW ratios W/W^* as a function of the metallicity $[\text{Fe}/\text{H}]$. Each row represents a selected line. Each panel of a row represents the W/W^* for a given effective temperature (3500, 4250 and 5250 K). Each colour of the W/W^* in a panel represents a surface gravity (red, green, blue and cyan for $\log g = 0.5, 1.0, 1.5$ and 2.0 dex respectively). The variations of W/W^* are not plotted when $W < 1 \text{ m}\text{\AA}$. We notice that MARCS model atmospheres are missing for $\log g = 0.5$, $T_{\text{eff}} \in [3500, 4500]$, and $[\text{Fe}/\text{H}] = -4$; and for $\log g = 0.5$, $T_{\text{eff}} \in [3500, 3900]$, and $[\text{Fe}/\text{H}] = -3.00$. The dotted line stands for no deviation from LTE. The dashed lines stand for a variation of $\pm 5\%$ of the W/W^* (corresponding to a variation of ± 0.04 dex of the $\Delta[\text{El}/\text{H}]$) in case of strong regime of the curve of growth theory. The solid lines stand for a variation of $\pm 10\%$ of the W/W^* (corresponding to a variation of ± 0.04 dex of the $\Delta[\text{El}/\text{H}]$) in case of weak regime of the curve of growth theory.

We show the most representative Mg I lines in Fig. A1:

- the 5183 Å W/W^* represents the Mg I b triplet lines at $\lambda\lambda$ 5167, 5172 and 5183;
- the 5711 Å W/W^* represents the similar behaviours of the $\lambda\lambda$ 4730, 5711 and 11828 lines;
- the 7657 Å W/W^* ;
- the 8806 Å W/W^* represents the similar behaviours of the $\lambda\lambda$ 4167, 4702, 5528 and 8806 lines that are issued from the $3p \ ^1P^o$;
- the 8923 Å W/W^* that is the counterpart of the 7657 Å in the singlet system;
- the 10312 Å W/W^* that is essentially formed in LTE.

We show the most representative Ca I lines in Fig. A2:

- the 4226 Å W/W^* represents the NLTE behaviour of a resonance line;
- the 4578 Å W/W^* ;
- the 5512 Å W/W^* represents the similar behaviour of the $\lambda\lambda$ 5512, 5867 and 7326 lines;
- the 6122 Å W/W^* represents the similar behaviour of the Ca I red triplet lines at $\lambda\lambda$ 6102, 6122 and 6162;
- the 6166 Å W/W^* represents the similar behaviour of the multiplet lines at $\lambda\lambda$ 6161, 6166, 6169.0 and 6169.6;
- the 6572 Å W/W^* represents the NLTE behaviour of an intercombination resonance line.

We show all the selected lines for the Ca II lines in Fig. A3.

APPENDIX B: W/W^* FOR THE LINES IN THE GAIA/RVS WAVELENGTH RANGE

We present the results of the NLTE computations and the polynomial fits as the evolution of the NLTE/LTE EW ratios W/W^* as a function of the metallicity $[\text{Fe}/\text{H}]$ for the Mg I, Ca I and Ca II lines in the Gaia/RVS wavelength range [8470, 8740] Å in Fig. B1 and B2. Each row represents an observed line, except for the quoted row at 8715 Å standing for the Ritz wavelength of the Mg I triplet at $\lambda\lambda$ 8710, 8712 and 8717. Each panel of a row represents the W/W^* for a given effective temperature (3500, 4250 and 5250 K), except for the Ca II 8542 and 8662 Å lines for which we used the following temperatures (3500, 4250 and 5000 K) in order to add polynomial fit of Starkenburg et al. (2010) on the panels. Each colour of the dots and the polynomial fits W/W^* in a panel represents a surface gravity (red, green, blue and cyan for $\log g = 0.5, 1.0, 1.5$ and 2.0 dex respectively).

This paper has been typeset from a $\text{\TeX}/\text{\LaTeX}$ file prepared by the author.

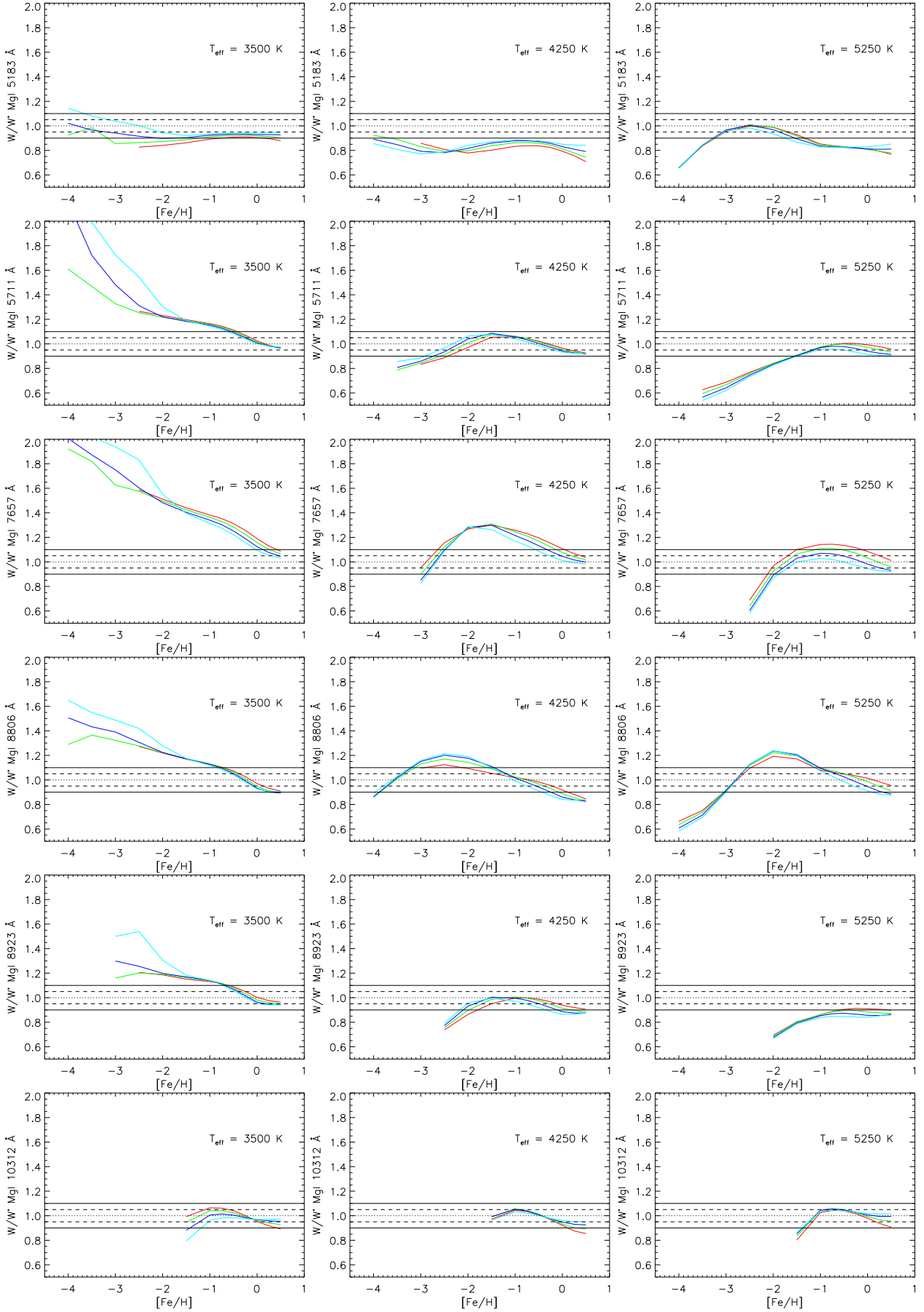


Figure A1. W/W^* for the selected Mg I lines as function of the stellar parameters (see Appendix A for details).

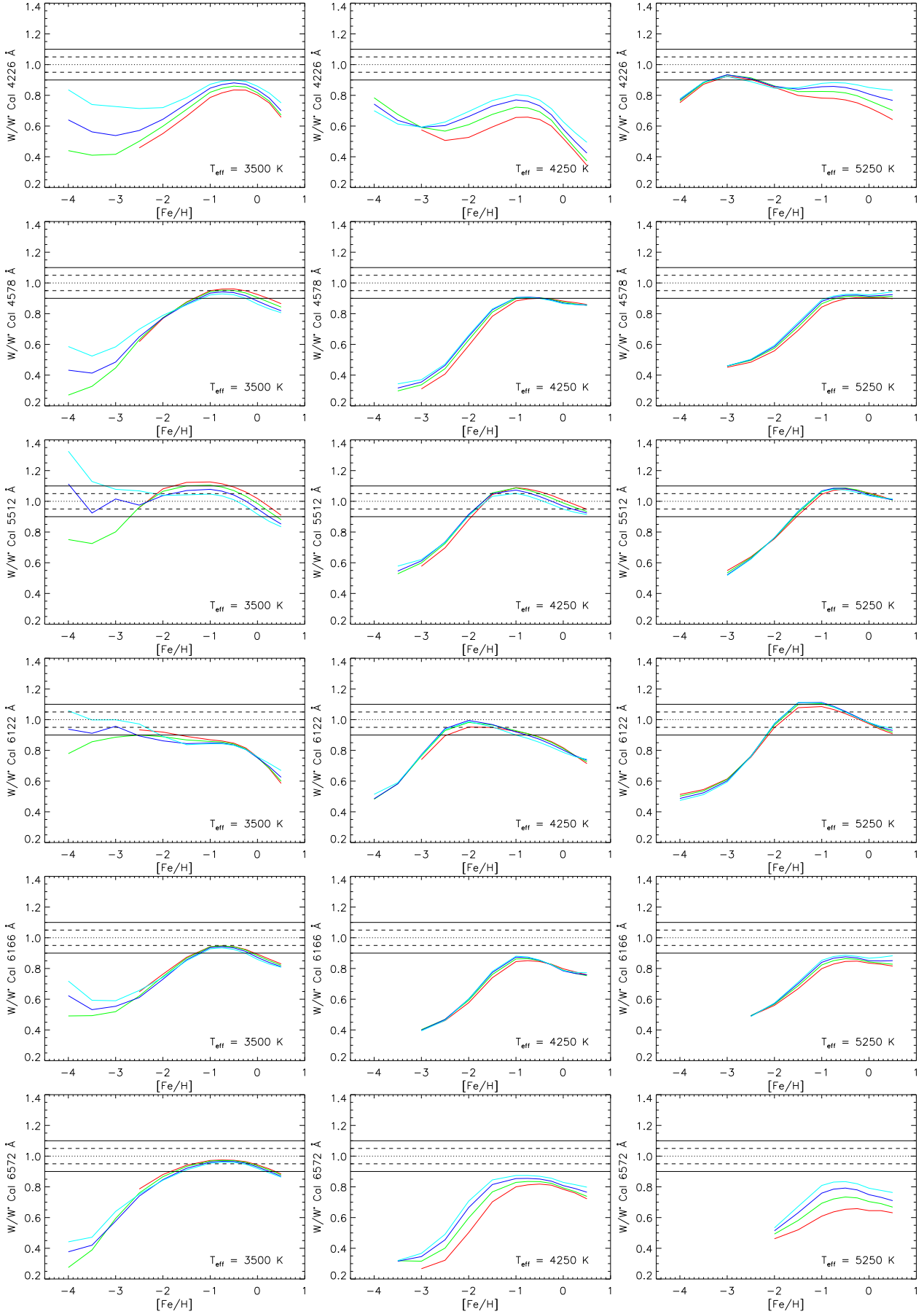


Figure A2. W/W^* for the selected Ca I lines as function of the stellar parameters (see Appendix A for details).

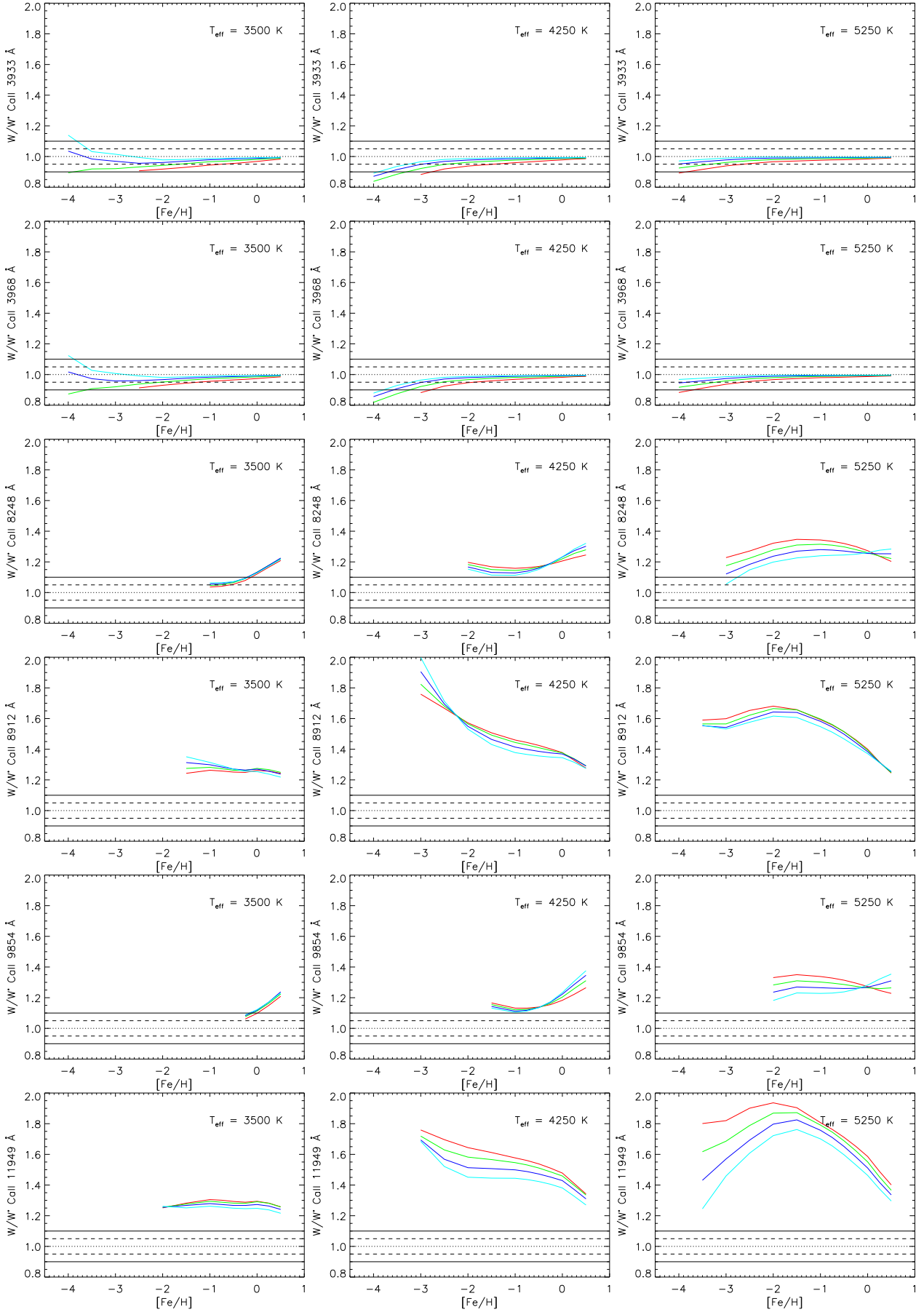


Figure A3. W/W^* for the selected Ca II lines as function of the stellar parameters (see Appendix A for details).

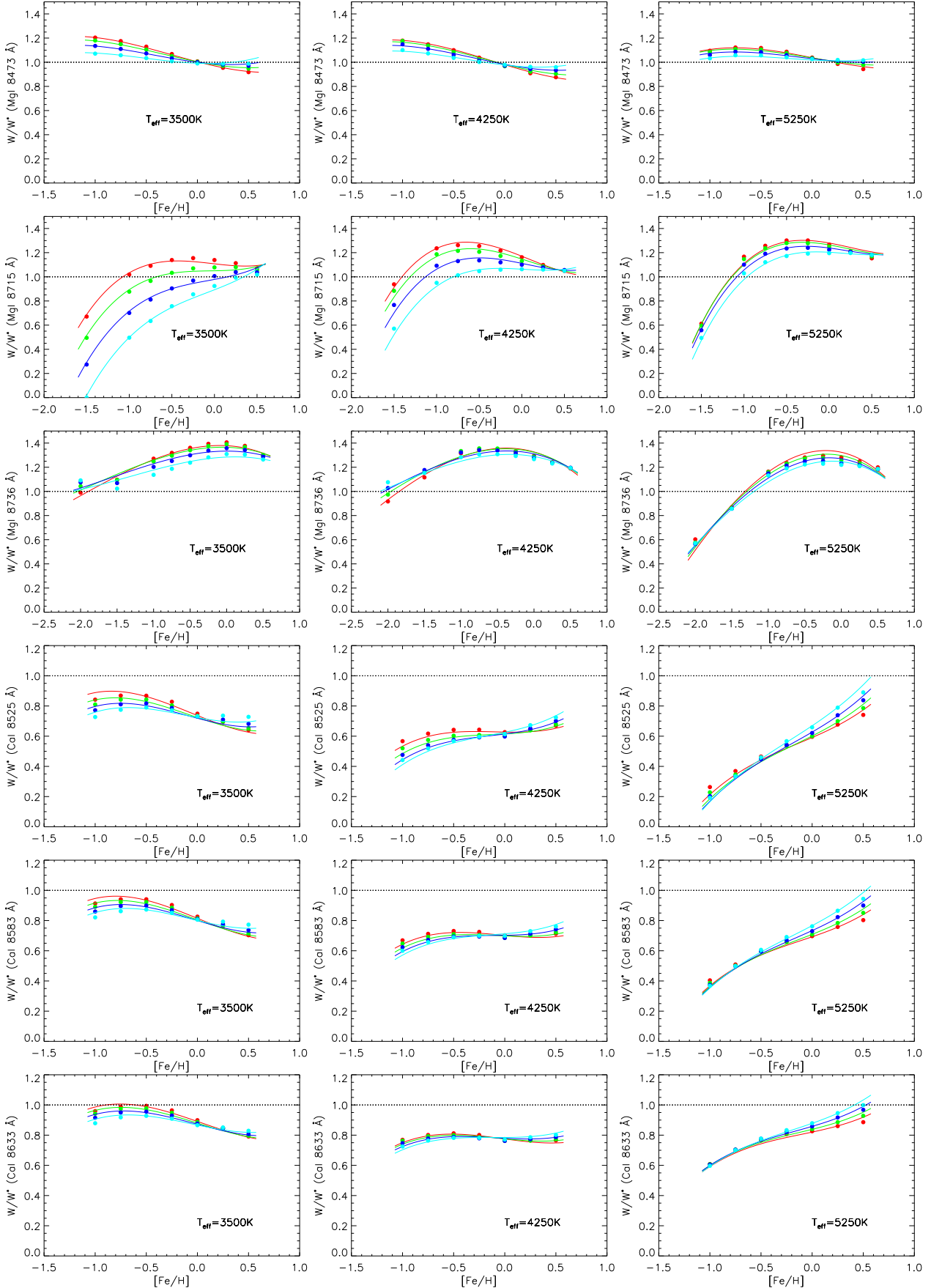


Figure B1. W/W^* for the *Gaia*/RVS Mg I and Ca I lines as function of the stellar parameters (see Appendix B for details).

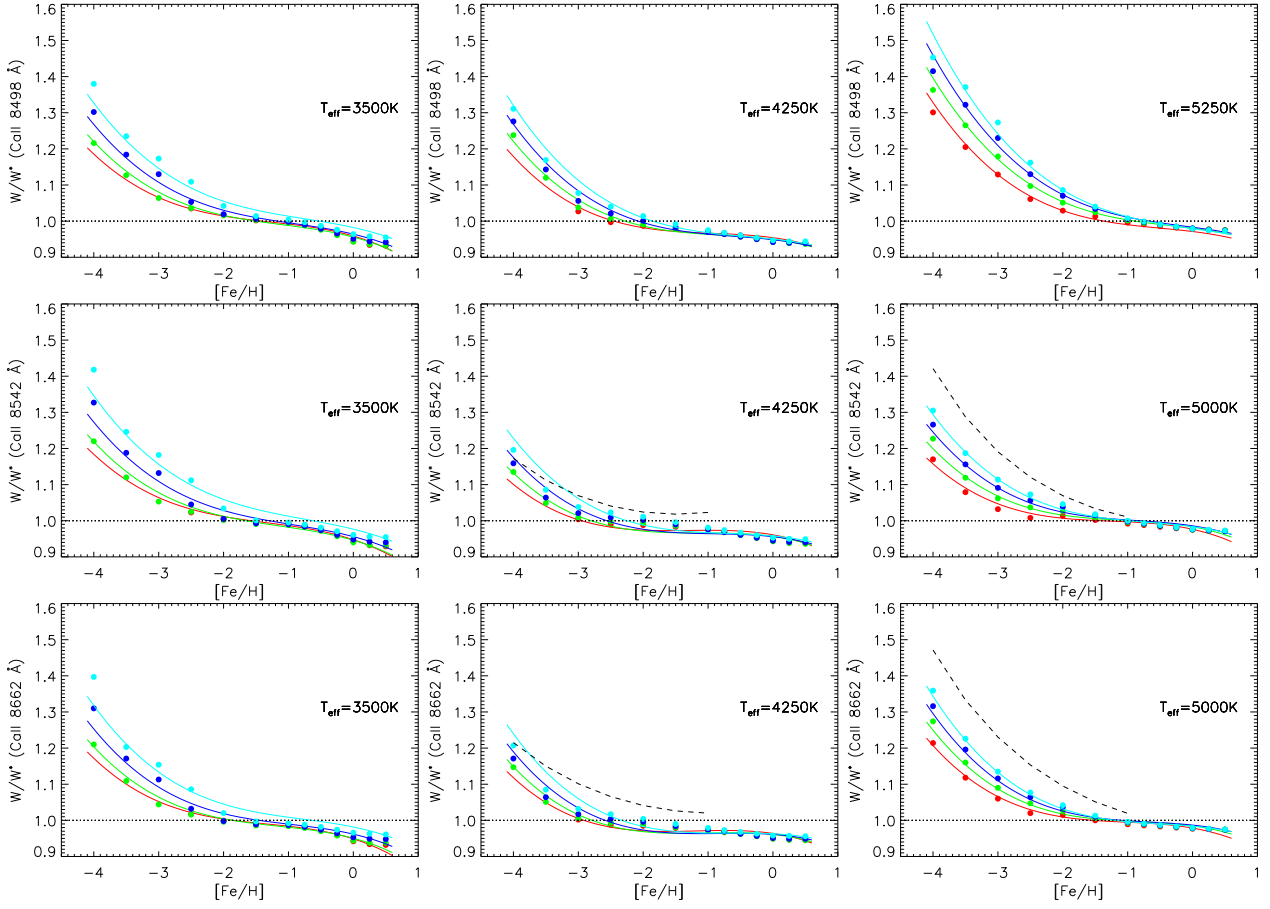


Figure B2. W/W^* for the *Gaia*/RVS Ca II lines as function of the stellar parameters (see Appendix B for details).